Synthesis, Structures, ^{1}H NMR Spectra, and Reactivity of Paramagnetic 46-Electron Trinuclear Clusters of the Form $(Cp^*M)_n(CpCo)_{3-n}(\mu_3\text{-}CO)_2$ (M = Co, Rh, Ir; n = 1, 2)

Craig E. Barnes,* Michelle R. Dial, and Jeffery A. Orvis

Department of Chemistry, University of Tennessee, Knoxville, Tennessee 37996

Donna L. Staley and Arnold L. Rheingold

Department of Chemistry, University of Delaware, Newark, Delaware 19716

Received September 20, 1989

The preparation, structures, and spectroscopic characterization of two new series of paramagnetic 46-electron, heterotrimetallic clusters are reported, $(Cp^*M)(CpCo)_2(CO)_2$ ($^*MCo_2$ series, M = Ir, **1**; Co, **4**; Rh **5**) and $(Cp^*M)_2(CpCo)(CO)_2$ ($^*M_2Co$ series, M = Co **6**; Rh **7**; Ir **8**). Their synthesis uses the bisethylene complex $CpCo(C_2H_4)_2$ to act formally as a latent source of the CpCo fragment, which adds to either $Cp^*M(CO)_2$ ($^*MCo_2$ series) or the preformed, unsaturated dinuclear complexes $[Cp^*M(\mu\text{-}CO)]_2$ ($^*M_2Co$ series). Their structures reflect an important aspect of the bonding within the triangular $M_3(CO)_2$ cores. In each case, the trinuclear core may be divided into a dinuclear fragment that interacts with a mononuclear fragment determined by the positions of the carbonyl ligands in the solid state. In the $^*M_2Co$ series, the two fragments are the original dinuclear precursor to which has been added a CpCo fragment. In the $^*MCo_2$ series the positions of the carbonyl ligands vary with the different metals involved. For M = Co and Rh the carbonyls bridge the CpCo–CoCp edge, while for M = Ir the carbonyl ligands bridge the Ir–Co bond. For both series, in every case where the carbonyl ligands remain primarily edge bridging ($\theta < 15°$, θ = canting of the carbonyls off the perpendicular to the plane of the metal atoms, $\theta = 60°$ for μ_3-carbonyls), a marked elongation of the bridged metal–metal bond is observed, as compared to the analogous bond in the parent dinuclear complex. In one case ($^*Rh_2Co$), where the carbonyl ligands are triply bridging in the solid state, the Rh–Rh bond shows no significant lengthening in the trinuclear complex as compared to the dinuclear parent, $[Cp^*Rh(\mu\text{-}CO)]_2$. These data are consistent with the results of an extended Hückel MO calculation on the hypothetical complex $(CpRh)_3(CO)_2$ as reported by Pinhas et al. (*Helv. Chim. Acta.* **1980**, *63*, 29–49), where an elongation of the carbonyl-bridged bond is predicted as a CpM fragment is added to such a dinuclear species, as is observed in both of the above series. Furthermore, this analysis predicts that this in-plane M–M antibonding orbital should rise in energy and become unoccupied as the carbonyl ligands assume triply bridging coordination geometries. This prediction is consistent with the behavior of $^*Rh_2Co$, which is the only complex with μ_3-carbonyls in the solid state. These calculations also indicate that the HOMO–LUMO separation should be small for these complexes. Consistent with this prediction is the observation of paramagnetically shifted ^{1}H NMR spectra, for which a general model involving thermal equilibria between singlet (S = 0) and triplet (S = 1) isomers of each complex is proposed. Complexes **1**, **6**, and **8** exhibit linear increasing shifts with increasing inverse temperature. Assuming a contact shift mechanism, the spin equilibria for complexes **4**, **5**, and **7** were modeled according to eq 1. The average enthalpy and entropy differences between the two isomers for these complexes are as follows: **4**, ΔH = 10.56 (5) kJ/mol; ΔS = 35 (4) J/(mol·K); **5**, 20 (2) kJ/mol, 45 (10) J/(mol·K); **7**, 8.2 (1) kJ/mol, 34 (1) J/(mol·K). Members of the $^*M_2Co$ series exhibit the interesting ability to exchange the dinuclear fragment $[Cp^*M(\mu\text{-}CO)]_2$ (M = Co, Rh, Ir) from within their core for a new dinuclear complex, thus producing one of the other members of this series. This reaction is catalyzed by ethylene. The mechanism is proposed to involve initial coordination of ethylene to the CpCo fragment followed by loss of the dinuclear complex. The resulting CpCo mono- or bisethylene species is then captured by a second dinuclear complex. These reactions underscore the isolobal analogies between the title complexes and an unsaturated, 16-electron CpM(ethylene) species. The relationship between these reactions and fundamental cluster building and degradation reactions is also discussed. The crystal data were as follows: **4**, monoclinic, $C2/c$, a = 15.254 (6) Å, b = 15.827 (5) Å, c = 8.341 (3) Å, β = 97.57 (3)° Z = 4, $R(F)$ = 3.5%; **5**, monoclinic, $P2_1/n$, a = 13.444 (7) Å, b = 11.342 (3) Å, c = 14.086 (7) Å, β = 107.11 (4)° Z = 4, $R(F)$ = 3.19%; **6**, orthorhombic, $Ccmm$, a = 10.197 (3) Å, b = 13.902 (6) Å, c = 17.851 (6) Å, Z = 4, $R(F)$ = 6.74%; **7**, orthorhombic, $Ccmm$, a = 10.292 (4) Å, b = 13.702 (4) Å, c = 18.544 (9) Å, Z = 4, $R(F)$ = 6.15%; **8**, orthorhombic, $Pnma$, a = 20.187 (6) Å, b = 15.779 (3) Å, c = 16.689 (4) Å, Z = 8, $R(F)$ = 5.35%.

Introduction

Since the discovery of the trinickel complex $(CpNi)_3(CO)_2$ by Fischer and Palm,[1] this class of trinuclear clusters has been the object of considerable study and has played an important role in understanding the properties of cluster complexes. The reasons for this are several-fold. Extensive structural studies[2] have produced a well-defined, highly symmetric structure type for these clusters. This information has subsequently been used in several theoretical investigations[3] from which has come a detailed picture of the metal–metal and metal–ligand interactions underlying the triangular metal array capped by two triply bridging ligands. A second, related area of interest has focused on the types of the capping ligands found in these complexes. The properties of a ligand interacting with several metal centers are of obvious importance in understanding the reactivity of organic species on metal surfaces and possibly of heterogeneous catalyst systems.[4]

(1) Fischer, E. O.; Palm, C. *Chem. Ber.* **1958**, *91*, 1725–1731. Hock, A. A.; Mills, O. S. In *Advances in the Chemistry of Coordination Compounds*; Kirschner, S., Ed.; MacMillan: New York, 1961; pp 640–648.

0276-7333/90/2309-1021$02.50/0

Of special note in this regard is the role the complex, $Co_3(\mu_3\text{-}CCH_3)(CO)_9$,[5,6] played in the identification of the μ_3-alkylidyne moiety as a product from the binding and activation of ethylene on platinum surfaces.[7] Finally, polynuclear cluster complexes often serve as catalyst precursors in reactions involving unsaturated mononuclear complexes.[8] Little is known, however, about the factors and mechanisms that govern the formation and degradation of cluster complexes and how these reactions might be tailored to produce new in situ type catalysts.[9]

More recently, several new strategies for the systematic synthesis of this type of trinuclear cluster have been developed. One such approach involves the reaction of a labile complex, which functions as a latent source of a reactive metal fragment, with a second mono- or polynuclear organometallic complex to produce a cluster of higher nuclearity:[8-10]

$$ML_n + M'L'_m \longrightarrow L_{n-1}M(L)M'L'_{m-1} + L'$$

In the course of the reaction, the ligands lost by the labile complex are replaced by new metal–metal bonds, bridging ligands, or an organometallic analogue to the ligand lost. The notions of isolobality developed by Hoffmann and co-workers[11] may be used in this context as a guide in the choice of which metal fragments and organometallic combinations may be combined to produce stable cluster complexes.[12]

We[13] have used this method to prepare several new heterotrinuclear complexes of the form $(CpCo)_n(Cp^*M)_{3-n}(CO)_2$[14] (M = Co, Rh or Ir; 1, 4–8). Herein we

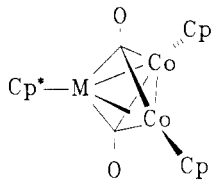

1: M = Ir

4: M = Co

5: M = Rh

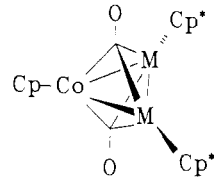

6: M = Co

7: M = Rh

8: M = Ir

describe the preparation and characterization of two complete series of complexes involving either one CpCo fragment interacting with the $[Cp^*M(\mu\text{-}CO)]_2$ fragment or a Cp*M fragment interacting with $[CpCo(\mu\text{-}CO)]_2$. These complexes distinguish themselves from previous examples in this area by exhibiting a much broader range of bridging carbonyl geometries than has been observed before. These complexes also exhibit an unanticipated set of thermal spin equilibria involving low-energy triplet states which have been characterized by variable-temperature NMR investigations. Furthermore, structural evidence and new reactivity patterns are described that permit these mixed-metal systems to be viewed as a mononuclear fragment interacting with a dinuclear species, similar to the synthetic strategy employed in their preparation. In particular, we describe here a novel binuclear exchange reaction between trinuclear clusters of these series that is catalyzed by ethylene. The relevance of these exchange reactions are discussed within the context of cluster metathesis reactions. A preliminary account of some aspects of this work has already appeared.[13b]

Results

A. Synthesis. The synthesis and structure of the first member of these series of complexes, $Cp^*Ir(CpCo)_2(\mu\text{-}CO)_2$ (1), have already been described.[13a] The methodology developed for this complex appears to be generally applicable to all the members of these series with one additional note. 1 may be prepared by the formal addition of a "CpCo" fragment (derived from the labile bisethylene complex $CpCo(C_2H_4)_2$,[15] **2**) to the preformed heterodinuclear complex $Cp^*Ir(\mu\text{-}CO)_2CoCp$,[13c] **3**. It is also possible to prepare 1 and the corresponding cobalt and rhodium analogues $Cp^*M(CpCo)_2(\mu\text{-}CO)_2$ (M = Co, **4**; Rh, **5**) directly from the mononuclear dicarbonyl complexes, $Cp^*M(CO)_2$, and 2 equiv of the bisethylene complex, **2** as summarized in Scheme I. Addition of the dicarbonyl complex to an excess of the bisethylene complex ensures that as the mixed-metal, dinuclear intermediate is formed, it immediately adds a second equivalent of "CpCo" to form the trinuclear product.[16]

(2) (a) Beyers, L. R.; Uchtman, U. A.; Dahl, L. F. *J. Am. Chem. Soc.* **1981**, *103*, 1942–1951. (b) Stenson, D. L.; Wei, C. H.; Dahl, L. F. *J. Am. Chem. Soc.* **1971**, *93*, 6027–6031. (c) Strouse, C. E.; Dahl, L. F. *Discuss. Faraday Soc.* **1969**, *No. 47*, 93–106. (d) Strouse, C. E.; Dahl, L. F. *J. Am. Chem. Soc.* **1971**, *93*, 6032–6041. (e) Beyers, L. R.; Uchtman, V. A.; Dahl, L. F. *J. Am. Chem. Soc.* **1981**, *103*, 1942–1951. (f) Uchtman, V. A.; Dahl, L. F. *J. Am. Chem. Soc.* **1969**, *91*, 3763–3769. (g) Vahrenkamp, H.; Uchtman, V. A.; Dahl, L. F. *J. Am. Chem. Soc.* **1968**, *90*, 3272–3273. (h) Bedard, R. L.; Rae, A. D.; Dahl, L. F. *J. Am. Chem. Soc.* **1980**, *108*, 5924–5932. (i) Bedard, R. L.; Dahl, L. F. *J. Am. Chem. Soc.* **1986**, *108*, 5933–5942. (j) Cirjak, L. M.; Huang, J.-S.; Zhu, Z.-H.; Dahl, L. F. *J. Am. Chem. Soc.* **1980**, *102*, 6623–6626.

(3) (a) Pinhas, A. R.; Albright, T. A.; Hofmann, P.; Hoffmann, R. *Helv. Chim. Acta* **1980**, *63*, 29–49. (b) Schilling, B. E. R.; Hoffmann, R. *J. Am. Chem. Soc.* **1979**, *101*, 3456–3467. (c) Elian, M.; Hoffmann, R. *Inorg. Chem.* **1975**, *14*, 1058–1076. (d) Rives, A. R.; Xiao-Zeng, Y.; Fenske, R. F. *Inorg. Chem.* **1982**, *21*, 2286–2294.

(4) (a) Monim, S. S.; Venus, D. Roy, D.; McBreen, P. H. *J. Am. Chem. Soc.* **1989**, *111*, 4106–4108. (b) Zheng, C.; Apeloig, Y.; Hoffmann, R. *J. Am. Chem. Soc.* **1988**, *110*, 749–774. (c) Muetteries, E. L.; Rhodin, T. N.; Band, E.; Brucker, Pretzer, W. R. *Chem. Rev.* **1979**, *79*, 91–137, and references therein.

(5) (a) Howard, M. W.; Kettle, S. F.; Oxton, I. A.; Powell, D. B.; Sheppard, N.; Skinner, P. *J. Chem. Soc., Faraday Trans. 2* **1981**, *77*, 397–404. (b) Skinner, P.; Howard, M. F.; Oxton, I. A.; Kettle, S. F. A.; Powell, D. B.; Sheppard, N. *J. Chem. Soc., Faraday Trans. 2* **1981**, *77*, 1203–1215.

(6) Other trinuclear systems containing a triply bridging alkylidyne group: (a) Herrmann, W. A.; Plank, J.; Guggolz, E.; Ziegler, M. L. *Angew. Chem., Int. Ed. Engl.* **1980**, *19*, 651–653. (b) Dimas, P. A.; Duesler, E. N.; Lawson, R. J.; Shapley, J. R. *J. Am. Chem. Soc.* **1980**, *102*, 7787–7789. (c) Fritch, J. R.; Vollhardt, K. P. C.; Thompson, M. R.; Day, V. W. *J. Am. Chem. Soc.* **1979**, *101*, 2768–2770.

(7) (a) Ibach, H.; Hopster, H.; Sexton, B. *Appl. Surf. Sci.* **1977**, *1*, 1–30. (b) Kesmodel, L. L.; Stair, P. C.; Baetzold, R. C.; Somorjai, G. A. *Phys. Rev. Lett.* **1976**, *36*, 1316–1319. (c) Gavezotti, A.; Simonetta, M. *Surf. Sci.* **1980**, *99*, 453–470. (d) Anderson, A. B.; Hubbard, A. T. *Surf. Sci.* **1980**, *99*, 384–391.

(8) Vahrenkamp, H. *Adv. Organomet. Chem.* **1983**, *22*, 169–208.

(9) Garrou, P. E. *Adv. Organomet. Chem.* **1984**, *23*, 95–129.

(10) See, for example: (a) Green, M.; Hankey, D. R.; Howard, J. A. K.; Louca, P.; Stone, F. G. A. *J. Chem. Soc., Chem. Commun.* **1983**, 757–758. (b) Bray, A. C.; Green, M. Hankey, D. R.; Howard, J. A. K.; Johnson, O.; Stone, F. G. A. *J. Chem. Soc., Chem. Commun.* **1985**, C12–C16. (c) Olson, W. L.; Stacy, A. M.; Dahl, L. F. *J. Am. Chem. Soc.* **1986**, *108*, 7646–7656.

(11) Hoffmann, R. *Angew. Chem., Int. Ed. Engl.* **1982**, *21*, 711–800, and references therein.

(12) Stone, F. G. A. *Angew. Chem., Int. Ed. Engl.* **1984**, *23*, 89–99.

(13) (a) Herrmann, W. A.; Barnes, C. E.; Zahn, T.; Ziegler, M. L. *Organometallics* **1985**, *4*, 172–180. (b) Barnes, C. E.; Dial, M. R. *Organometallics* **1988**, *7*, 782–784. (c) Hörlein, R.; Herrmann, W. A.; Barnes, C. E.; Weber, C. *J. Organomet. Chem.* **1987**, *321*, 257–272. (d) Barnes, C. E.; Orvis, J. A.; Staley, D. L.; Rheingold, A. L.; Johnson, D. C. *J. Am. Chem. Soc.* **1989**, *111*, 4992–4994.

(14) To facilitate the discussion of the composition and structural attributes of these complexes the following abbreviations will be used in the text: Cp = η^5-cyclopentadienyl; Cp* = η^5-pentamethylcyclopentadienyl; Cp(*) = either Cp or Cp*; *M = (η^5-Cp*)M, (M = Co, Rh or Ir); M (alone) = (η^5-Cp)M.

(15) (a) Jonas, K. *Angew. Chem., Int. Ed. Engl.* **1985**, *24*, 295–311. (b) Jonas, K.; Deffense, E.; Habermann, D. *Angew. Chem., Int. Ed. Engl.* **1983**, *22*, 716–717; *Angew. Chem. Suppl.* **1983**, 1005–1016.

(16) Related studies in our laboratories indicate that these mixed-metal, mixed-Cp/Cp* dinuclear intermediates also metathesize with themselves (unpublished results).

Scheme I

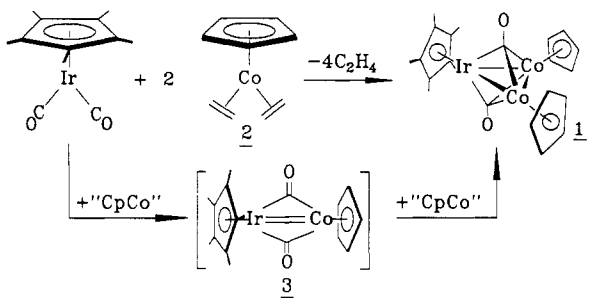

Table I. Carbonyl Infrared Stretching Frequencies (THF)

dinuclear precursor[a]	ν(CO), cm^{-1}	derived trinuclear	ν(CO), cm^{-1}	$\Delta\nu$
$Cp^*Ir(\mu\text{-}CO)_2CoCp$	1738	$^*IrCo_2$ (1)	1680	−58
$CpCo(\mu\text{-}CO)_2CoCp$	1785	$^*CoCo_2$ (4)	1707	−78
$CpCo(\mu\text{-}CO)_2CoCp$	1785	$^*RhCo_2$ (5)	1705	−80
$Cp^*Co(\mu\text{-}CO)_2CoCp^*$	1747	$^*Co_2Co$ (6)	1698	−49
$Cp^*Rh(\mu\text{-}CO)_2RhCp^*$	1736	$^*Rh_2Co$ (7)[b]	1692	−44
$Cp^*Ir(\mu\text{-}CO)_2IrCp^*$	1690	$^*Ir_2Co$ (8)	1678, 1900[c]	−12

[a] Based on edge bridging positions of carbonyl ligands in the trinuclear product. [b] Carbonyls triply bridging in the solid state. [c] Terminal carbonyl stretch observed in solution or KBr. This phenomenon is under further investigation (see ref 18).

Members of the other series of trinuclear clusters $(Cp^*M)_2CpCo(\mu\text{-}CO)_2$ (M = Co **6**; Rh **7**; Ir **8**) are prepared from the preformed dinuclear precursors and at least 1 equiv of the bisethylene complex, **2**.

The use of a mixed-solvent system (ether/hexane) simplifies the workup and purification of these air-sensitive complexes. Ether is necessary to solubilize the dinuclear precursor complexes and appears to facilitate the reaction. Ethylene evolved during the course of the reaction is removed along with ether by brief exposure of the reaction mixture to vacuum. As the solvent system becomes enriched in hexane, the trinuclear products precipitate as microcrystalline solids in yields of 70–90%.

B. IR and ^{1}H NMR Characterization. The IR stretching frequencies for the carbonyl ligands[17] in these trinuclear complexes are summarized in Table I and are compared to the stretches for the corresponding dinuclear precursors $[Cp^{(*)}M(\mu\text{-}CO)]_2$. In every case, a single carbonyl stretch is observed that is 10–80 cm^{-1} lower than the corresponding stretch observed for the dinuclear precursor. The six trinuclear complexes may be divided into two series on the basis of the magnitude of change in the carbonyl stretching frequency in forming a trinuclear complex from a dinuclear precursor. Members of the first series (**1**, **4**, **5**) which contain two CpCo fragments, exhibit the largest shifts (60–80 cm^{-1}) in the CO stretching frequencies, whereas the second series (**6**–**8**), having only one CpCo fragment, exhibits smaller changes (10–50 cm^{-1}). A reduction of the carbonyl stretching frequency is indicative of a change from μ_2- to μ_3-bridging character for carbonyl ligands. In several of the complexes, only partial canting of the bridging carbonyls from a μ_2- to μ_3-coordination mode is observed in their solid-state structures.

The proton NMR spectra for these complexes are extraordinary; although the valence-electron count is even (46), the signals for the ring protons of the Cp ligands and the methyl hydrogens of the Cp* ligands in these complexes are shifted far upfield of their normal positions (approximately 2 and 5 ppm, respectively). In most cases

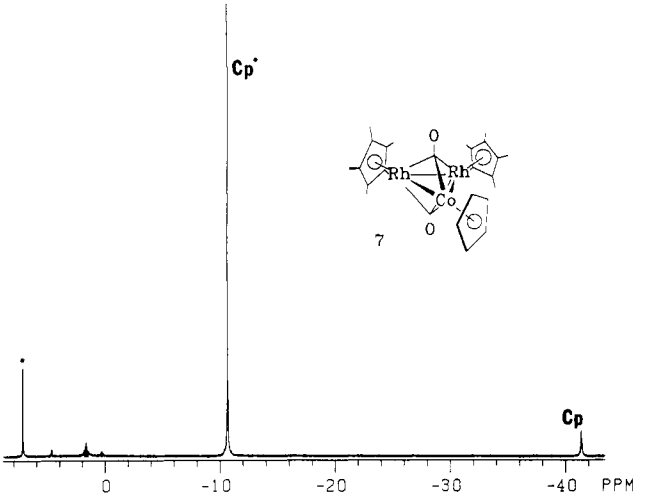

Figure 1. ^{1}H NMR spectrum of **7** (* = solvent, (C_6D_6); T = 25 °C).

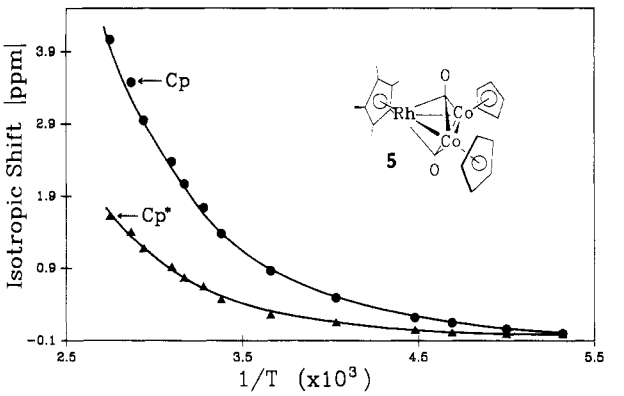

Figure 2. Temperature dependence of the isotropic ^{1}H shifts for **5**. Smooth curve through the data is based on least-squares fit to eq 1.

both signals are found upfield of TMS. The spectrum of **7** may be taken as representative and is shown in Figure 1. By integration, the Cp ligand is accounted for in the signal at −41.9 ppm, while the signal for *both* the Cp* ligands is observed at −10.8 ppm. Both signals are highly temperature dependent but show little dependence on sample concentration or solvent (C_6D_6, toluene-d_8, THF-d_8). The line width for the Cp* signals observed for these complexes varies from 5 to 20 Hz, while for the Cp signals the line widths fall in the range of 20–100 Hz.

The proton signals for complexes **1**,[13a] **6**,[13b] and **8**[18] are displaced further upfield from their respective diamagnetic frequency ranges as the temperature is lowered. For these three complexes, plots of shift vs inverse temperature are linear (apparent Curie behavior). In contrast, the Cp and Cp* signals associated with **5** exhibit the opposite temperature dependence, decreasing and become temperature independent (paramagnetic shift → 0) below −75 °C as shown in Figure 2. Finally, the signals for **4** and **7** exhibit maxima in their shift versus inverse temperature plots.[13b] This behavior is illustrated for complex **7** in Figure 3. The smooth curves through the data in both figures are best fits to eq 1 presented in the Discussion section.

(17) The spectra for these complexes do not exhibit any unusual shifts due to solvent or concentration.

(18) The Cp and Cp* signals for complex **8** exhibit coalescence behavior, each splitting into two unequal peaks below −60 °C, in addition to the temperature dependences described in the text. This behavior is currently under further investigation. Both above and below the coalescence region, though, the shifts resume their linear dependence with inverse temperature, albeit with slightly different slopes.

Table II. Crystal Data for 4–8

	$Cp^*Co(CpCo)_2(CO)_2$ (4)	$Cp^*Rh(CpCo)_2(CO)_2$ (5)	$(Cp^*Co)_2CpCo(CO)_2$ (6)	$(Cp^*Rh)_2CpCo(CO)_2$ (7)	$(Cp^*Ir)_2CpCo(CO)_2$ (8)
formula	$C_{22}H_{25}O_2Co_3$	$C_{22}H_{25}O_2Co_2Rh$	$C_{27}H_{35}O_2Co_3$	$C_{27}H_{35}O_2CoRh_2$	$C_{27}H_{35}O_2CoIr_2$
formula wt	498.239	542.211	568.374	656.318	834.91
cryst syst	monoclinic	monoclinic	orthorhombic	orthorhombic	orthorhombic
space group	$C2/c$	$P2_1/n$	$Ccmm$	$Ccmm$	$Pnma$
a, Å	15.254 (6)	13.444 (7)	10.197 (3)	10.292 (4)	20.187 (6)
b, Å	15.827 (5)	11.342 (3)	13.902 (6)	13.702 (4)	15.779 (3)
c, Å	8.341 (3)	14.086 (7)	17.851 (6)	18.554 (9)	16.689 (4)
β, deg	97.57 (3)	107.11 (4)	90	90	90
V, Å^3	1996 (1)	2052 (1)	2530 (1)	2616 (2)	5316 (2)
Z	4	4	4	4	8
D(calc), g cm^{-3}	1.66	1.75	1.49	1.67	2.09
μ (Mo Kα), cm^{-1}	24.7	23.8	19.6	18.5	112.3
T, K	296	296	296	296	296
cryst size, mm	0.17 × 0.18 × 0.33	0.23[3]	0.23[3]	0.15 × 0.2 × 0.30	0.20 × 0.20 × 0.25
hkl collected	±20,+21,+11	±16,+13,+17	+13,+17,+22	+14,+18,+25	+24,+19,+20
scan type	Wyckoff	Wyckoff	Wyckoff	Wyckoff	Wyckoff
2θ scan limits, deg	4–55	4–48	4–50	4–55	4–48
rflns coll	2587	3615	2495	3273	4645
indpdnt rflns	2301	3220	1212	1613	4334
obsd rflns ($F_o \geq 5\sigma$)	1777	2463	815	1234	2417
T(max)/T(min)	no corr	1.10	1.29	1.37	3.75
data/parameter	9.5	10.0	7.8	16.0	9.1
R(F), %	3.50	3.19	6.74	6.15	5.35
R(wF), % $[w^{-1} = \sigma^2(F_o) + gF_3^2]$	4.67	4.44	8.78	8.85	5.50
GOF	1.113	1.028	1.893	1.866	1.265
Δ/σ max	0.056	0.017	0.072	0.123	0.086
$\epsilon(\rho)$ max, e Å^{-3}	0.397	0.557	0.818	1.224	1.45

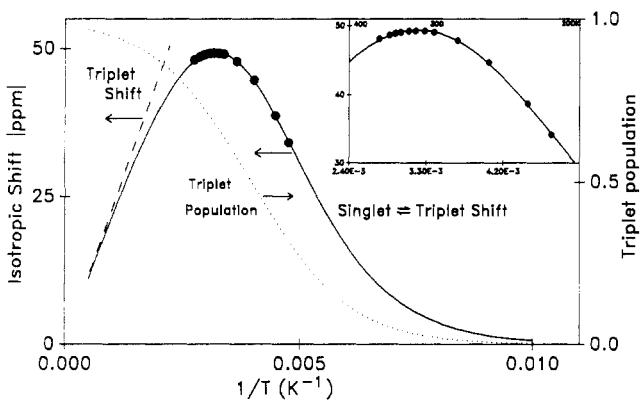

Figure 3. Temperature dependence of the isotropic ^{1}H shift for the Cp signal of **7**. Solid lines through data are based on least-squares fit to eq 1. See text for discussion of dotted and dashed curves.

Discussion

General Description of the Solid-State Structures of Complexes 1 and 4–8. The general structure type exhibited by the $M_3(CO)_2$ core of these complexes is a triangular array of metal atoms capped on either side by a single carbonyl ligand.[19] Within these series, the full range of doubly to triply bridging carbonyl coordination modes is exhibited. Each metal has either an η^5-Cp or -Cp* ligand coordinated perpendicular to the metal-atom plane. As described in the Experimental Section, disorder in the Cp and Cp* rings causes ambiguity in the definition of these ligands. However, there is no disorder observed in the more relevant $M_3(CO)_2$ cores. Two views of complexes 4–8 are presented in Figures 4–9. (The structure of 1 has already been described.[13a]) Figure 10 shows the packing scheme for the two independent molecules (A and B) in the asymmetric unit for 8. Selected bond distances and angles for these complexes are given in Tables II–VI.

(19) Complexes 4–8 all crystallize as discrete molecules with no unusually short or significant intermolecular contacts.

Scheme II

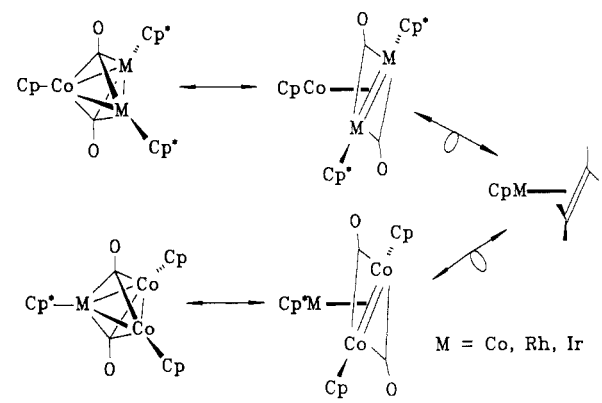

Scheme III

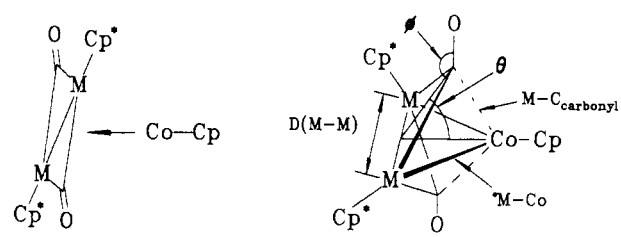

Each structure may be described as an unsaturated dinuclear complex to which a CpCo or Cp*M fragment has been added. This dinuclear fragment ($[Cp^{(*)}M(\mu\text{-}CO)]_2$) is isolobal with ethylene, and as shown in Scheme II, these trinuclear complexes are isolobal with the corresponding 16-electron $Cp^{(*)}M$(ethylene) species.

Using this fragment analysis, two types of changes take place when a CpCo fragment is brought up to the face of a $[Cp^*M(\mu\text{-}CO)]_2$ species: those relating to perturbations suffered by the $\overline{M(\mu\text{-}CO)_2M}$ core of the dinuclear species and those that are indicative of new, interfragment interactions. Pinhas et al. have described a similar model in their extended Hückel analysis of the hypothetical complex, $Cp_3Rh_3(CO)_2$;[3a] Scheme III is an adaptation of

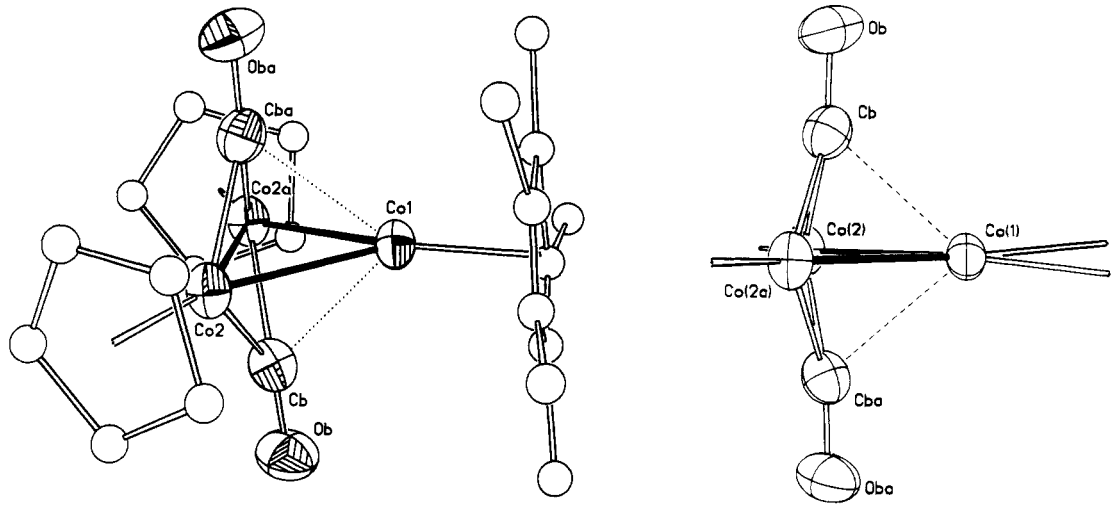

Figure 4. Two views of the molecular structure of $Cp^*Co(CpCo)_2(CO)_2$, **4**. A crystallographic 2-fold axis contains Co(1) and bisects the Co(2)–Co(2a) vector, causing rotational disorder in the Cp* ring (one orientation was arbitrarily selected for depiction).

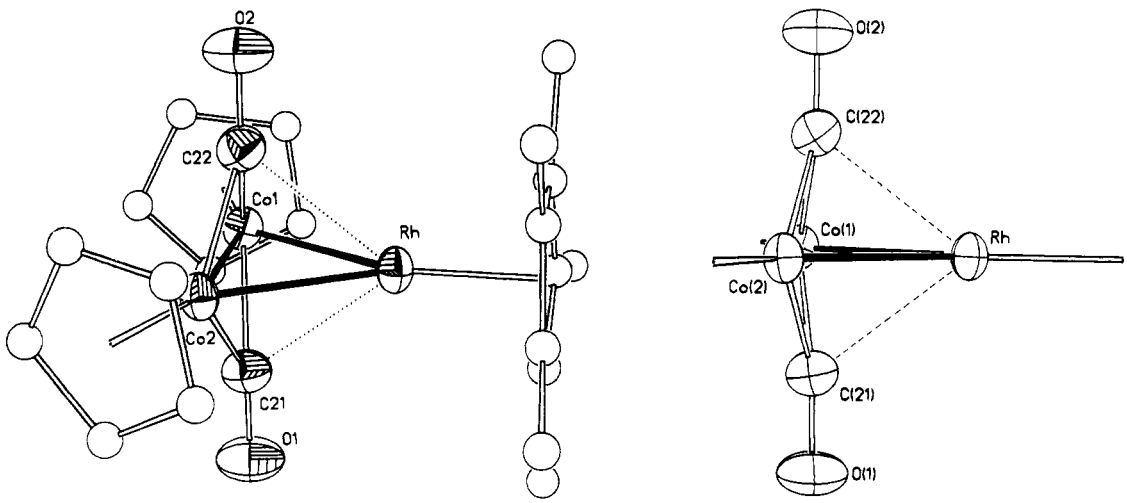

Figure 5. Two views of the molecular structure of $Cp^*Rh(CpCo)_2(CO)_2$, **5**.

one of the figures presented in this report. The following structural parameters are used in the analysis of the $*MCo_2$ series: The extent to which the carbonyl ligands cant over the plane of the metal atoms toward the incoming fragment is measured by the angle θ and by the $C_{carbonyl}$–Co distance. The angle ϕ measures the degree to which the carbonyl oxygen bends away from the incoming CpCo fragment as the CO group moves toward it. Changes in metal–metal bonding interactions are compared with two parameters: (1) the lengths of the two new Co–M bonds; (2) the change in the length of the M-M bond between the original dinuclear parent and this bond in the corresponding trinuclear product. Table VII summarizes these parameters for complexes 1 and 4–8.

A. Structures within the $(Cp^*M)_2CpCo(\mu\text{-}CO)_2$ ($*M_2Co$) Series (6–8). Metal–Cobalt Separations. As a CpCo fragment is added to the face of the planar $[M(\mu\text{-}CO)]_2$ core, two new Co–M bonds are formed. A common structural feature for all the members of this series is the very short Cp*M–CoCp distances within the metal triangle (column 6, Table VII). These atom separations are between 0.2 and 0.3 Å shorter than the sum of the appropriate covalent radii.[20] A somewhat more revealing basis for comparison is found in the analogous mixed-metal systems having formal single or double metal–metal bonds within similar ligand environments. The methylene bridged Ir–Co bond (2.624 (1) Å, entry 17, Table VIII), which represents a formal single bond between the metal atoms, is 0.15 Å longer than the average Ir–Co separation in **8** (2.473 Å). The complex $Cp^*Ir(\mu\text{-}CO)_2CoCp$, which possesses a formal double Ir–Co bond[21] of 2.45 (1) Å, is only 0.02 Å shorter than the Ir–Co separation in **8**. The only other Ir–Co bond known within a similar ligand environment is that reported for $Cp^*Ir(CpCo)_2(\mu\text{-}CO)_3$ (entry 18, Table VIII). In this complex each of the M–M bonds supports a bridging carbonyl ligand, all of which are found

(20) Covalent radii (Å): Co 1.26; Rh 1.35; Ir 1.37; C 0.77; O 0.77. From *Inorganic Chemistry*; Porterfield, W. W., Ed.; Addison-Wesley: Reading, MA; p 168.

(21) There is some question concerning the degree to which the bridging ligands influence the separation of the two metal atoms in complexes of the form $[CpM(\mu\text{-}CO)]_2$. Extended Hückel calculations by Pinhas and Hoffmann[22a] could not account for the invariance of the separation between the metal atoms when the total electron count was increased, causing metal–metal antibonding orbitals to be filled. These authors speculated that contributions from the bridging ligands (CO and NO) influence the final equilibrium separation of metal atoms. More recently, Schugart and Fenske[22b,c] have reexamined these systems using the Fenske–Hall molecular orbital method.[23] Not only do these calculations support the single- and double-bond valence formalisms, but they also identify more clearly that metal–ligand interactions are indeed important in determining the overall ordering of molecular orbitals (and thus the metal–metal separations) in this type of complex.

(22) (a) Pinhas, A. R.; Hoffmann, R. *Inorg. Chem.* **1979**, *18*, 654–658. (b) Schugart, K. A.; Fenske, R. F. *J. Am. Chem. Soc.* **1986**, *108*, 5094–5100. (c) Schugart, K. A.; Fenske, R. F. *J. Am. Chem. Soc.* **1986**, *108*, 5100–5104. (d) Griewe, G. L.; Hall, M. B. *Organometallics* **1988**, *7*, 1923–1930.

(23) (a) Hall, M. B.; Fenske, R. F. *Inorg. Chem.* **1972**, *11*, 768–775. (b) Fenske, R. F. *Prog. Inorg. Chem.* **1972**, *21*, 179–208.

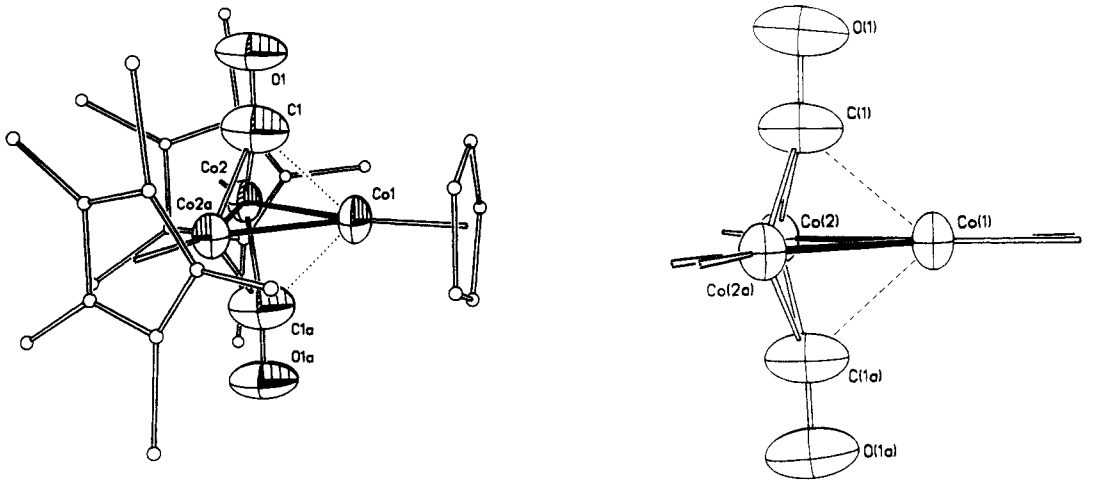

Figure 6. Two views of the molecular structure of $(Cp^*Co)_2CpCo(CO)_2$, **6**. The molecule possesses two crystallographic mirror planes, one containing the plane of metal atoms, the other contains Co(1) and the midpoint of the Co(2)–Co(2a) vector and is perpendicular to the first plane. The disorder caused by these planes could be only partially resolved for the Cp and Cp* rings (see text).

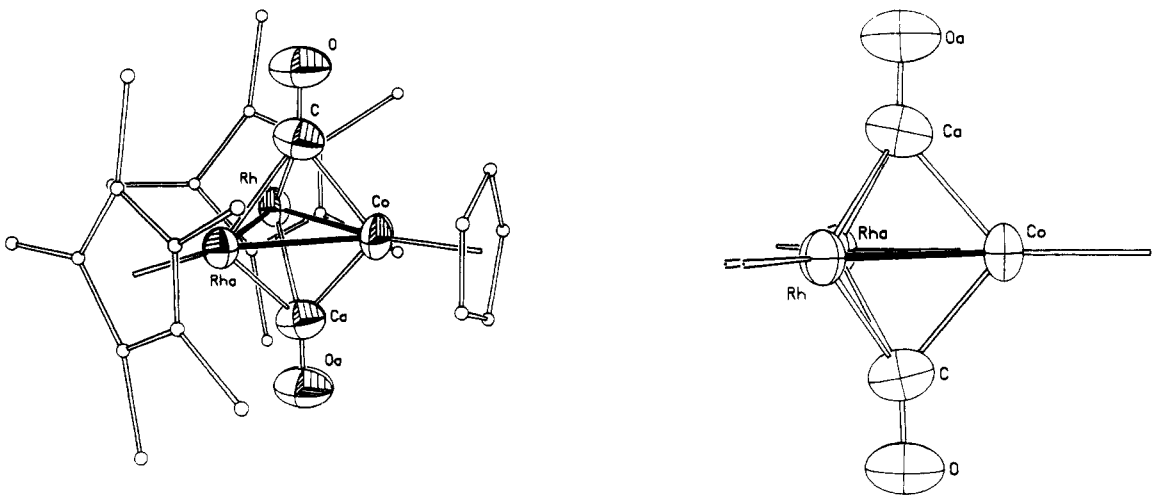

Figure 7. Two views of the molecular structure for $(Cp^*Rh)_2CpCo(CO)_2$, **7**. See caption for Figure 6 for comments about disorder.

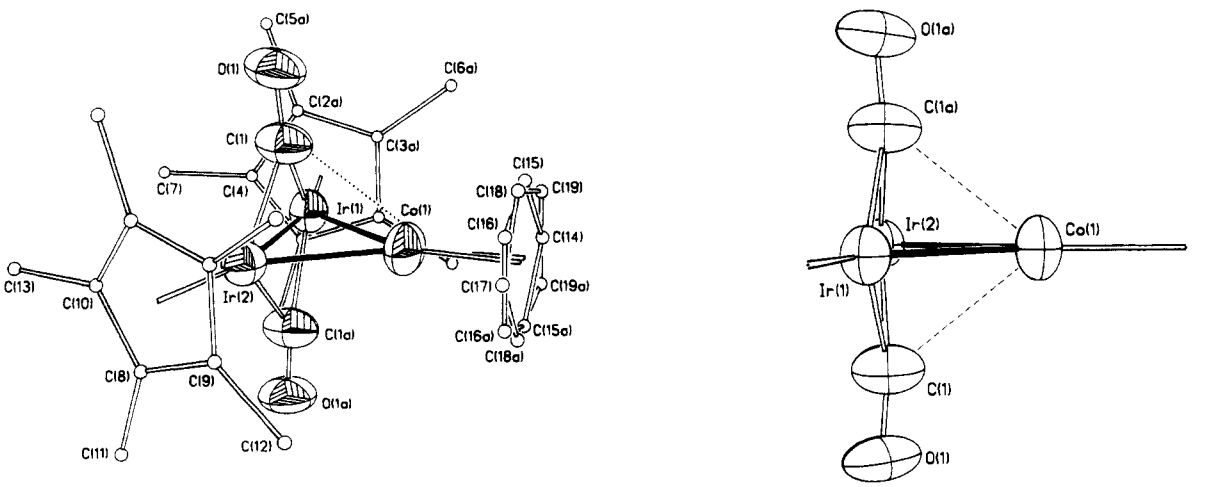

Figure 8. Two views of the molecular structure and numbering scheme for $(Cp^*Ir)_2CpCo(CO)_2$, **8** molecule A: the dotted line denotes long-distance Co–CO interaction; thermal ellipsoids drawn at 40% level. The Co(1) Cp ring is disordered over two coplanar but not coaxial sites.

on the same side of the plane of the metal atoms. The average of the Ir–Co separations in this trinuclear complex is 2.54 Å. This value is 0.06 Å longer than that observed in **8**.

The unbridged *Co–Co bond in **6** (2.335 (2) Å) is bracketed by the few distances reported that correspond to formal single (2.50 Å, average of entries 6 and 7, Table VIII) and double (2.33 Å, average of entries 1 and 2, Table VIII) Co–Co bonds in related complexes. Likewise, the *Rh–Co separation in **7** is slightly larger (+0.065 Å) than the value reported for a Rh–Co double bond in Cp*Rh-(μ-CO)CoCp* (entry 15, Table VIII). Two other complexes that also contain the $[Cp^*Rh(\mu\text{-CO})]_2$ fragment are $(Cp^*Rh_3)(\mu\text{-}CO_2)$ and $Mo(CO)_5[Cp^*Rh(\mu\text{-CO})]_2$ (entries 10 and 11, Table VIII). The different metals involved in these complexes make comparisons less exact, but the Rh–Mo

Table III. Selected Bond Lengths (Å) and Angles (deg) for 4 and 5

4		5	
Co(1)-Co(2)	2.305 (1)	Rh-Co(1)	2.433 (1)
Co(2)-Co(2a)	2.405 (1)	Rh-Co(2)	2.431 (1)
		Co(1)-Co(2)	2.426 (1)
Co(1)-Cb	2.160 (3)	Rh-C(21)	2.322 (6)
Co(2)-Cb	1.884 (3)	Rh-C(22)	2.319 (5)
		Co(1)-C(21)	1.896 (5)
		Co(1)-C(22)	1.884 (6)
		Co(2)-C(21)	1.872 (6)
		Co(2)-C(22)	1.884 (5)
Co(1)-CNT(1)[a]	1.679 (7)	Rh-CNT (3)	1.815 (6)
Co(2)-CNT(2)	1.725 (7)	Co(1)-CNT(1)	1.725 (5)
		Co(2)-CNT(2)	1.720 (5)
CNT(1)-CNT(1a)	0.457 (6)		
Cb-Ob	1.174 (4)	C(21)-O(1)	1.188 (7)
		C(22)-O(2)	1.182 (7)
Co(2)-Co(1)-Co(2a)	62.9 (1)	Co(1)-Rh-Co(2)	59.8 (1)
Co(1)-Co(2)-Co(2a)	58.5 (1)	Rh-Co(1)-Co(2)	60.0 (1)
		Rh-Co(2)-Co(1)	60.1 (1)
Co(2)-Co(1)-Cb	49.8 (1)	Co(1)-Rh-C(21)	46.9 (1)
Co(1)-Co(2)-Cb	61.1 (1)	Co(1)-Rh-C(22)	46.6 (2)
		Co(2)-Rh-C(21)	46.3 (1)
		Co(2)-Rh-C(22)	46.7 (1)
		Rh-Co(1)-C(21)	63.5 (2)
		Rh-Co(1)-C(22)	63.5 (2)
		Co(2)-Co(1)-C(21)	49.5 (2)
		Co(2)-Co(1)-C(22)	49.9 (1)
		Rh-Co(2)-C(21)	63.8 (2)
		Rh-Co(2)-C(22)	63.5 (2)
		Co(1)-Co(2)-C(21)	50.4 (1)
		Co(1)-Co(2)-C(22)	49.9 (2)
Co(1)-Cb-Ob	129.2 (3)	Co(1)-C(21)-O(1)	139.2 (5)
Co(2)-Cb-Ob	139.3 (3)	Co(1)-C(22)-O(2)	139.2 (4)
		Co(2)-C(21)-O(1)	138.7 (4)
		Co(2)-C(22)-O(2)	138.1 (5)
		Rh-C(21)-O(1)	126.7 (4)
		Rh-C(22)-O(2)	127.8 (5)
Co(1)-CNT(1)-CNT-(1a)	82.2 (3)	Co(1)-Rh-CNT(3)	150.9 (3)
		Co(2)-Rh-CNT(3)	149.2 (3)
		Rh-Co(1)-CNT(1)	140.7 (2)
		Co(2)-Co(1)-CNT(1)	159.3 (3)
		Rh-Co(2)-CNT(2)	140.3 (2)
		Co(1)-Co(2)-CNT(2)	159.5 (2)
CNT(1)-Co(1)-CNT-(1a)	15.6 (3)		

[a] CNT denotes the centroid of a Cp or Cp* ring.

separation is quite close to the sum of the covalent radii in contrast to the short Rh–Co separation observed in **7**. The trirhodium complex exhibits both long and short Rh–Rh separations, which are correlated to the positions of the edge-bridging carbonyl ligands, similar to complexes **6** and **8**. The short M–CoCp distances observed in **6–8** are indicative of strong metal–metal interactions. Both the trirhodium complex and complexes **6–8** are unsaturated, 46-electron species. The molybdenum complex is a 48-electron complex and exhibits a much larger Mo–Rh distance.

Perturbations of the $[Cp^*M(\mu\text{-}CO)]_2$ Fragment. The structures of all the original dinuclear complexes are known (Table VIII). The separation between the metal atoms in the $^*\overline{M(\mu\text{-}CO)_2M}^*$ unit after addition of the CpCo fragment is dependent on the position of the bridging carbonyls in the solid state. The carbonyl ligands in **6** and **8** remain primarily edge bridging over the original *M–M* edge (M = Co, $\theta = 74°$; M = Ir, $\theta = 84°$) as compared to a fully triply bridging carbonyl (μ_3-CO, $\theta = 60°$). In both of these complexes the *M–M* separation is appreciably larger than the separation in the respective dinuclear precursor. The changes in this bond length for the dif-

Table IV. Selected Bond Lengths (Å) and Angles (deg) for 6 and 7

6		7	
Co(1)-Co(2)	2.335 (2)	Co-Rh	2.469 (2)
Co(2)-Co(2a)	2.373 (3)	Rh-Rh(a)	2.560 (1)
Co(1)-C(1)	2.135 (17)	Co-C	1.925 (14)
Co(2)-C(1)	1.891 (11)	Rh-C	2.124 (11)
Co(1)-CNT(1)*	1.838 (20)	Co-CNT(1)	1.784 (15)
Co(2)-CNT(2)	1.721 (16)	Rh-CNT(2)	1.869 (19)
CNT(1)-CNT(1a)	0.770 (11)	CNT(1)-CNT(1a)	0.727 (12)
CNT(2)-CNT(2a)	0.358 (10)	CNT(2)-CNT(2a)	0.218 (12)
C(1)-O(1)	1.186 (17)	C-O	1.129 (15)
Co(2)-Co(1)-Co-(2a)	61.1 (1)	Rh-Co-Rh(a)	62.4 (1)
Co(1)-Co(2)-Co-(2a)	59.5 (1)	Co-Rh-Rh(a)	58.8 (1)
Co(2)-Co(1)-C(1)	49.8 (3)	Rh-Co-C	56.2 (3)
Co(1)-Co(2)-C(1)	59.6 (5)	Co-Rh-C	48.8 (4)
Co(1)-C(1)-O(1)	129.8 (14)	Co-C-O	137.7 (14)
Co(2)-C(1)-O(1)	138.9 (5)	Rh-C-O	134.4 (7)
Co(1)-CNT(1)-CNT(1a)	77.9 (11)	Co-CNT(1)-CNT(1a)	78.3 (13)
Co(2)-CNT(2)-CNT(2a)	83.7 (13)	Rh-CNT(2)-CNT(2a)	82.0 (14)
Co(2)-CNT(2a)-CNT(2)	84.4 (13)	Rh-CNT(2a)-CNT(2)	91.4 (13)
CNT(1)-Co(1)-CNT(1a)	24.2 (11)	CNT(1)-Co-CNT(1a)	23.4 (13)
CNT(2)-Co(2)-CNT(2a)	11.9 (11)	CNT(2)-Rh-CNT(2a)	6.6 (11)

Table V. Selected Bond Distances (Å) for Complex 8

molecule A		molecule B	
Ir(1)-Ir(2)	2.658 (2)	Ir(3)-Ir(3a)	2.634 (2)
Ir(1)-Co(1)	2.132 (4)	Ir(3)-Co(2)	2.475 (4)
Ir(2)-Co(1)	2.480 (5)		
Ir(1)-C(1)	2.018 (22)	Ir(3)-C(21)	1.998 (24)
Ir(2)-C(1)	2.017 (21)	Ir(3)-C(22)	1.952 (27)
Co(1)-C(1)	2.442 (25)	Co(2)-C(21)	2.43 (3)
		Co(2)-C(22)	2.44 (3)
C(1)-O(1)	1.170 (27)	C(21)-O(21)	1.21 (4)
		C(22)-O(22)	1.25 (4)
Ir(1)-CNT(1)	1.911 (18)	Ir(3)-CNT(3)	1.874 (18)
Ir(2)-CNT(2)	1.903 (18)		
Co(1)-CNT(A)	1.85 (2)	Co(2)-CNT(C)	1.89 (3)
Co(1)-CNT(B)	1.85 (2)		
CNT(A)-CNT(B)	0.204		

Table VI. Selected Bond Angles (deg) for Complex 8

molecule A		molecule B	
Ir(1)-Co(1)-Ir(2)	65.0 (1)	Ir(3)-Co(2)-Ir(3a)	64.3 (1)
Ir(1)-Ir(2)-Co(1)	57.2 (1)	Ir(3)-Ir(3a)-Co(2)	57.8 (1)
Ir(2)-Ir(1)-Co(1)	57.8 (1)		
Ir(1)-C(1)-O(1)	138.0 (18)	Ir(3)-C(21)-O(21)	138.3 (7)
Ir(2)-C(1)-O(1)	137.2 (17)	Ir(3)-C(22)-O(22)	136.7 (8)
Co(1)-C(1)-O(1)	133.0 (20)	Co(2)-C(21)-O(21)	128.0 (24)
		Co(2)-C(22)-O(22)	130.5 (22)
Ir(1)-C(1)-Ir(2)	82.4 (8)	Ir(3)-C(21)-Ir(3a)	82.5 (12)
Ir(1)-C(1)-Co(1)	66.3 (7)	Ir(3)-C(22)-Ir(3a)	84.9 (14)
Ir(2)-C(1)-Co(1)	66.8 (7)	Ir(3)-C(21)-Co(2)	67.2 (9)
		Ir(3)-C(22)-Co(2)	67.5 (10)
C(1)-Ir(1)-C(1a)	96.8 (12)	C(21)-Ir(3)-C(22)	95.7 (10)
C(1)-Ir(2)-C(1a)	96.8 (12)	C(21)-Co(2)-C(22)	73.9 (11)
C(1)-Co(2)-C(1a)	76.3 (11)		
CNT(1)-Ir(1)-Co(1)	137.2 (3)	CNT(3)-Ir(3)-Ir(3a)	159.2 (4)
CNT(1)-Ir(1)-Ir(2)	165.1 (4)	CNT(3)-Ir(3)-Co(2)	143.0 (4)
CNT(2)-Ir(2)-Ir(1)	163.0 (4)	CNT(C)-Co(2)-Ir(3)	147.5 (4)
CNT(2)-Ir(2)-Co(1)	139.7 (3)		
CNT(A)-Co(1)-Ir(1)	150.6 (11)		
CNT(B)-Co(1)-Ir-(1)	144.2 (11)		
CNT(A)-Co(1)-Ir(2)	144.4 (11)		
CNT(B)-Co(1)-Ir-(2)	150.7 (11)		

Table VII. Selected Structural Parameters for Trinuclear Complexes 1 and 4–8 Based on Scheme III

complex	D(M-M), Å	θ, deg	ϕ, deg	Δ(M-M),[a] Å	D(M-Co), Å	D(M-$C_{carbonyl}$), Å
1[b]	2.527 (1)	85	174 (175)[c]	+0.076 (Ir-Co)	2.473 (1) (Ir-Co) 2.359 (1) (Co-Co)	2.41[d]
4	2.405 (1)	77	169 (167)	+0.083 (Co-Co)	2.305 (2) (Co-Co)	2.16
5	2.426 (1)	81	172 (169)	+0.104 (Co-Co)	2.432 (1) (Rh-Co)	2.32
6	2.373 (3)	74	165.5 (164)	+0.035 (Co-Co)	2.335 (2) (Co-Co)	2.14
7	2.560 (1)	60	151 (150)	−0.004[e] (Rh-Rh)	2.469 (2) (Rh-Co)	1.93
8						
molecule A	2.658 (2)	84	169.2 (174)	+0.108 (Ir-Ir)	2.47[d] (Ir-Co)	2.44
molecule B	2.634 (2)	83 85	173 (173) 171 (175)	+0.084 (Ir-Ir)	2.475 (4) (Ir-Co)	2.43[d]

[a] Difference in bond length between the carbonyl-bridged M-M bond in the trinuclear complexes listed here and the free dinuclear complex corresponding to this fragment within each particular trinuclear complex. Values for the dinuclear complexes chosen for each comparison are listed in Table VIII: 1, entry 18; 4, 5, entry 1; 6, entry 2; 7, entry 8; 8, entry 15. [b] Data from ref 13a. [c] Numbers in parentheses are the angles that correspond to a rigorous perpendicular orientation of the C–O bond to the plane of the metal atoms given the observed canting angle, θ. [d] Average of two values. [e] Carbonyl ligands triply bridging in the solid state. Rh–Rh bond used for comparison.

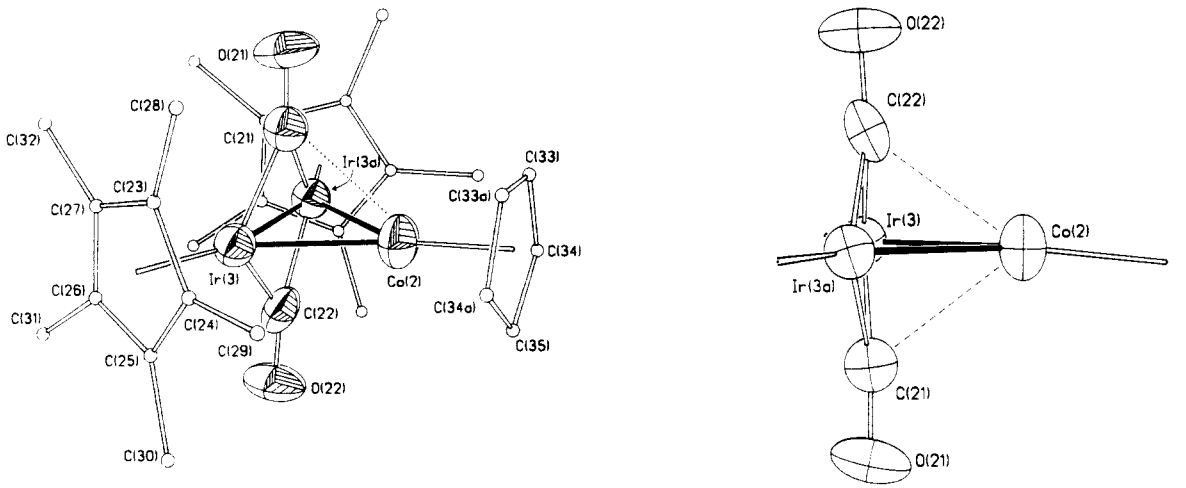

Figure 9. Molecular structure and numbering scheme for $(Cp^*Ir)_2CpCo(CO)_2$, 8 molecule B: long-distance Co–carbonyl interaction is represented by the dotted line; thermal ellipsoids drawn at 40% level.

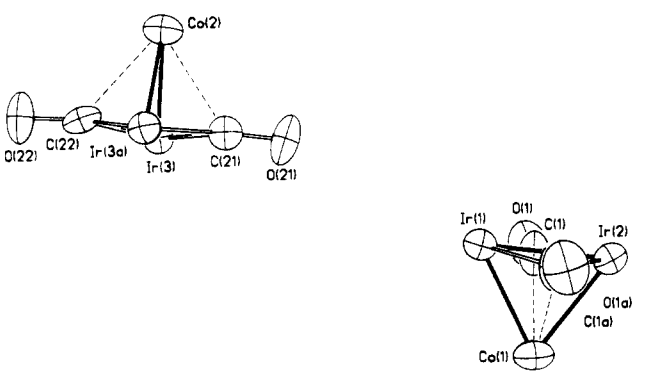

Figure 10. Packing diagram of $(Cp^*Ir)_2CpCo(CO)_2$ as viewed along *b* axis showing orientation of the molecules (A and B) on two distinct, perpendicular crystallographic mirror planes.

ferent dinuclear–trinuclear combinations are summarized in column 5 of Table VII. In **8** the elongation of this bond is among the largest observed for any pair of dinuclear parent–trinuclear products in either trinuclear series, $D(\text{Ir–Ir})_{\text{dinuclear}}$ = 2.55 Å (entry 13, Table VIII) → $D(\text{Ir–Ir})_{\text{trinuclear}}$ = 2.65 Å (average) (+0.1 Å). The Ir–Ir separation in **8** is now closer to that observed for a formal, single Ir–Ir bond (entry 14, Table VIII).

For complex **6**, the separation of the two cobalt atoms changes from 2.338 Å (entry 2, Table VIII) in the dinuclear parent to 2.373 Å (+0.035 Å) in the trinuclear product. This distance remains closer to that observed in the original dinuclear complex (where a formal Co–Co double bond exists) than to similar complexes that have formal Co–Co single bonds (entries 6 and 7, Table VIII). This change is similar to what has been observed for the one-electron reduction of the parent dinuclear complex (entries 1–4, Table VIII). In these instances the additional electron is thought to occupy a Co–Co antibonding orbital.

In marked contrast to these observations the carbonyl ligands assume fully triply bridging coordination geometries in **7** and the Rh–Rh bond distance is observed to be slightly (but not significantly) *smaller* than that observed in the original dirhodium parent (entry 8, Table VIII). The platinum complex $Pt[Cp^*Rh(\mu\text{-}CO)_2RhCp^*]_2$ (entry 12, Table VIII) and the molybdenum and trirhodium complexes described earlier all contain the same $[Cp^*Rh(\mu\text{-}CO)]_2$ fragment found in **7**. In all of these cases the carbonyls bridging the Rh–Rh bond remain almost perpendicular to the $PtRh_2$, $MoRh_2$, or Rh_3 planes, and the bridged Rh–Rh distance is considerably enlarged compared to the original dinuclear complex. Thus in the $*M_2Co$ series, the separation (and by inference the bonding) of the two metal atoms originally bridged by the carbonyl ligands is strongly linked to the approach of these ligands toward the unique CpCo fragment and a fully triply bridging geometry.

The $C_{carbonyl}$–M distances observed in these complexes fall into two categories: those that are a part of the original dinuclear species and those corresponding to the unique $C_{carbonyl}$–CoCp interaction. In the first case, all the M–C separations are similar to those observed for the parent dinuclear complexes. Given the lengthening observed in the bridged M–M bonding in complexes **6** and **8**, the

Table VIII. M–M Bond Distances in Selected Organometallic Complexes

entry	complex	M–M, Å	ref
	Co–Co		
1	$[CpCo(\mu\text{-}CO)]_2$	2.322 (2)	*a*
2	$[Cp^*Co(\mu\text{-}CO)]_2$	2.338 (2)	*b*
3	$[AsPh_4]^+[CpCp(\mu\text{-}CO)]_2^{\bullet-}$	2.364 (2)	*b, c*
4	$Na[2,2,2\ crypt]^+[Cp^*Co(\mu\text{-}CO)]_2^{\bullet-}$	2.372 (1)	*b*
5	$(Cp^*Co)_2(\mu\text{-}CO)(\mu\text{-}CH_2)$	2.320 (1)	*d*
6	$[Cp^*Co(CO)]_2(\mu\text{-}CH_2)$	2.502 (2)	*e*
7	$[Cp'Co(CO)]_2(\mu\text{-}CH_2)$ ($Cp' = C_5H_4Me$)	2.497 (1)	*f*
	Rh–Rh		
8	$[Cp^*Rh(\mu\text{-}CO)]_2$	2.564 (1)	*g*
9	$(Cp^*Rh(CO)_2(\mu\text{-}CH_2)$	2.672 (1)	*h*
10	$(Cp^*Rh)_3(\mu\text{-}CO)_2$	2.639 (2) 2.562 (av)	*i*
11	$Mo(CO)_5[Cp^*Rh(\mu\text{-}CO)]_2$	2.623 (1) (Rh–Rh)	*j*
12	$Pt([Cp^*Rh(\mu\text{-}CO)]_2)_2$	2.618 (2) (Rh–Rh)	*k*
	Ir–Ir		
13	$[Cp^*Ir(\mu\text{-}CO)]_2$	2.55[l]	*m*
14	$(Cp^*Ir(CO))_2(\mu\text{-}CH_2)$	2.689 (1)	*m*
	Mixed-Metal Systems		
15	$Cp^*Rh(\mu\text{-}CO)_2CoCp^*$	2.4040 (5)	*g*
16	$Cp^*Ir(\mu\text{-}CO)_2CoCp$	2.46 (1)	*n*
17	$Cp^*Ir(\mu\text{-}CH_2)(CO)_2CoCp$	2.624 (1)	*n*
18	$Cp^*Ir(\mu\text{-}CO)_3(CoCp)_2$	2.54 (av) (Ir–Co)	*n*

[a] Stella, S.; Floriani, C.; Chiesi-Villa, A.; Guastini, C. *New J. Chem.* **1988**, *12*, 621–631. [b] Cirjak, L. M.; Ginsburg, R. E.; Dahl, L. F. *Inorg. Chem.* **1982**, *21*, 940–957. [c] Shore, N. E.; Ilenda, C. S.; Bergman, R. G. *J. Am. Chem. Soc.* **1977**, *99*, 1781–1787. [d] Halbert, T. R.; Leonowicz, M. E.; Maydonovitch, D. J. *J. Am. Chem. Soc.* **1980**, *102*, 5101–5102. [e] Herrmann, W. A.; Bauer, C.; Huggins, J. M.; Pfisterer, H.; Ziegler, M. L. *J. Organomet. Chem.* **1983**, *258*, 81–99. [f] Theopold, K. H.; Bergman, R. G. *J. Am. Chem. Soc.* **1983**, *105*, 464–475. [g] Green, M.; Hankey, D. R.; Howard, J. A. K.; Louca, P.; Stone, F. G. A. *J. Chem. Soc., Chem. Commun.* **1983**, 757–758. [h] Herrmann, W. A.; Krüger, C.; Goddard, R.; Bernal, I. *J. Organomet. Chem.* **1977**, *140*, 73–89. [i] Reference 10b,c. [j] Barr, R. D.; Green, M.; Howard, J. A. K.; Marder, T. B.; Stone, F. G. A. *J. Chem. Soc., Chem. Commun.* **1983**, 759–760. [k] Green, M.; Howard, J. A. K.; Pain, G. N.; Stone, F. G. A. *J. Chem. Soc. Dalton Trans.* **1982**, 1327–1331. [l] Estimated standard deviation not given. [m] Heinekey, D. M.; Michelle, S. T.; Schulte, G. K. *Organometallics* **1989**, *8*, 1241–1241. [n] Reference 13c.

carbonyl ligands must move closer to that M–M bond to preserve, more or less, the M–C bond distances. The distances in the latter case are, with the exception of the triply bridging case (complex **7**), consistently quite larger than models cited. This large atom separation (0.1–0.3 Å larger than the sum of covalent radii) poses the question as to how significant an interaction exists between the CpCo fragment and these ligands. The results of Pinhas et al.[3a] indicate that the angle ϕ (Scheme III) is directly related to the degree of interaction of the carbonyl ligand with the third metal. In every case in the series under consideration, no matter how slight the canting of the carbonyl ligands over the plane of the metal atoms, the C–O bond tilts back (closing ϕ) so as to maintain an almost perpendicular orientation to the plane of the metal atoms, (column 4, Table VII). The correlation of the canting of the carbonyl ligands toward the CpCo unit with the perpendicular orientation of this ligand is structural evidence for some interaction of these edge bridging ligands with the CpCo fragment, even when the distance separating the two atoms is quite large.

B. Structures within the $Cp^*M(CpCo)_2(CO)_2$ ($^*MCo_2$) Series (1,[13a] 4, and 5). The members of this series are synthesized from the corresponding $Cp^*M(CO)_2$ and 2 equiv of the bisethylene complex **2**. In each case, the carbonyl ligands are best described as edge bridging with only a slight canting of these ligands toward the opposite metal atom. Surprisingly, the carbonyl ligands in complexes **4** and **5** are observed bridging the Co–Co edge opposite the Cp*M unit to which they were originally bound. In complex **1**, however, the carbonyl ligands remain associated with the Cp*Ir unit, bridging one of the Ir–Co bonds in the complex. This difference between complexes **4**, **5**, and **1** may be rationalized by the better back-bonding ability of iridium (5d valence orbitals) as compared to rhodium and cobalt (4d and 3d valence orbitals). In complex **1**, the strength of the Ir–carbonyl interaction is large enough to cause the carbonyl ligands to remain bound to the iridium atom in the solid state. In the case of **5** the bonding to the cobalt atoms of the $[CpCo(\mu\text{-}CO)]_2$ fragment appears to be stronger than the $Rh\text{–}C_{carbonyl}$ interaction, bridging or otherwise. It should be noted, however, that the carbonyl ligands in **1** are fluxional in solution.[13a] Thus, solid-state interactions are significant in determining the final position of the carbonyls in this complex.

In Scheme III, where the angles and distances are redefined by the positions of the bridging carbonyl ligands, the average angle θ for this series is 81° with a variance of 4°. As observed for the $^*M_2Co$ series, the carbonyl-bridged M–M bond experiences a marked elongation in the trinuclear species as compared to the appropriate dinuclear precursor. In the case of **1** the Ir–Co bond is 0.076 Å longer that the corresponding distance in **3**. For **4** and **5** the elongation of the Co–Co bond over what is observed in $[CpCo(\mu\text{-}CO)]_2$ is 0.083 and 0.104 Å, respectively. These metal–metal separations are midway between those observed for formal M–M double and M–M single bonds in similar ligand environments.

The Cp*Co–CoCp distance in **4** and the average Rh–Co distance in **5** are both quite short, presumably reflecting strong metal–metal interactions between the dinuclear fragment and mononuclear fragment within these and all other members of these series. The bending back of the carbonyl oxygen with the canting of this ligand over the plane of the metals is similar to the members in the previous series. The C–O bond vector remains virtually perpendicular to the plane of the metals in all cases.

The solid-state structures of these complexes reveal what we will show is an important feature of their underlying electronic structure. The edge-bridging nature of the carbonyl ligands in all but one of these complexes provides a natural division of the $M_3(CO)_2$ core into a dinuclear fragment containing the carbonyl ligands and the remaining $Cp^{(*)}M$ fragment. In the one exception where the carbonyl ligands become fully triply bridging, further studies concerning dinuclear exchange reactions will be presented that support its inclusion in this model. The short M–M distances between the di- and mononuclear fragments and long separations of the carbonyl carbons from the unique metal–$Cp^{(*)}$ fragment indicate that the dominant interactions between the two fragments are direct metal–metal interactions. In all cases where the carbonyl ligands remain edge-bridging, the way in which these fragments interact causes a marked lengthening of the bond between the metal atoms in the dinuclear fragment. These structural changes observed for the $M_3(CO)_2$ core appear to be caused by the intricate interplay of orbital interactions and solid-state effects that influence the final positions of the carbonyl ligands in these complexes.

^{1}H NMR Spectra. Chemical Shifts. The unusual paramagnetic shift behavior observed in the ^{1}H NMR spectra of these complexes may be explained qualitatively by a structural isomerism that is tied to a change in spin state. This well-known phenomenon has been observed

Table IX. Spin Equilibrium Parameters and Hyperfine Coupling Constants[a] According to Eq 3

complex	parameter	Cp	Cp*
4	$\gamma_0 K_i$,[a] Hz	−2.85 (1) × 10^6	−1.81 (6) × 10^5
	ΔH, kJ/mol	10.51 (6)	10.6 (5)
	ΔS, J/(mol·K)	31.1 (1)	39 (2)
	Δ^b_{diamag}, ppm	5.94[c]	2.0[d]
5	$\gamma_0 K_i$	−9.6 (3) × 10^6	−1.4 (2) × 10^5
	ΔH	17.9 (4)	22.3 (7)
	ΔS	34 (4)	56 (4)
	δ_{diamag}	5.08[e]	0.88[e]
7	$\gamma_0 K_i$	−1.98 (2) × 10^6	−4.98 (3) × 10^5
	ΔH	8.2 (1)	8.20 (8)
	ΔS	32.9 (7)	35.3 (4)
	δ_{diamag}	3.98[c]	2.0[d]

[a] $K_i = -A_i\gamma_e\beta S(S+1)/6S\gamma_H k$. All NMR spectra referenced to a proton resonance frequency of 200.01 MHz. [b] Reference diamagnetic shift. [c] Calculated from least-squares fit; see text. [d] Estimated diamagnetic shift; see text. [e] Experimentally measured, limiting diamagnetic shift value.

in many mononuclear transition-metal complexes[24] and more recently was described by Olson et al.[10c] for the trinuclear complex $(Cp^*Co)_3(CO)_2$. In these cases and here, one of the two isomers involved in the equilibrium is a singlet ($S = 0$) complex and the other a triplet ($S = 1$) complex containing two unpaired electrons. In this situation, the contact contribution to the isotropic shift, $\Delta H_i/H$ (hertz) is given by eq 1.

$$\left(\frac{\Delta H_i}{H}\right)_{\text{contact}} = \frac{-A_i\gamma_e g\beta S(S+1)}{6S\gamma_H k}\,\frac{1}{T}[e^{\Delta G/RT}+1]^{-1} \qquad (1)$$

A_i is the hyperfine coupling constant between a specific nucleus and the unpaired spins in the complex, and ΔG is the free energy difference between the singlet and triplet forms of the molecule. The limiting diamagnetic behavior exhibited by complex **5** (Figure 2) is clear evidence that the singlet state is lower in energy than the triplet state. The inset to Figure 3 shows that over the temperature range of the data (363–183 K) an excellent fit[25] to eq 1 is obtained for the maximum observed in the temperature dependence of the Cp signal for complex **7**.[26] Extrapolating in both directions illustrates the overall nature of the dependence of shift on temperature predicted by eq 1. The maximum in the paramagnetic shift may be understood in terms of the characteristics of the triplet state modulated by its increasing population with increasing temperature. These two factors are shown in Figure 3 as dashed curves.

Given the limited temperature range studied, independent measurement of the hyperfine coupling constant (limiting high-temperature behavior) and thermodynamic parameters is impossible from these data alone. Also, neither the magnitude of the anisotropy in the g values nor the limiting low-temperature diamagnetic shifts for these complexes are known. The fit parameter corresponding to the hyperfine coupling constant is therefore left in a general form K_i, where $K_i = -A_i\gamma_e\beta S(S+1)/6S\gamma_H k$. Good fits to the data were obtained for complexes **4**, **5**, and **7**. The hyperfine coupling constants (K_i) and enthalpy and entropy values from the fits are summarized in Table IX.

Qualitative agreement between the fit parameters for the Cp and Cp* signals is obtained for each complex except **4**. In all of the least-squares fits a high degree of cross correlation between the fit parameters was indicated by the correlation matrix. The nature of this correlation of variables was further investigated by exploring how the fit changed when the reference diamagnetic shifts were allowed to vary.[27] The least-squares fits for the Cp signals all converged to reasonable values of the diamagnetic reference offset (given in Table IX), while the fits to the Cp* signals converged to unrealistic (both positive and negative) values. Furthermore, the least-squares fit parameters were found to be highly sensitive and correlated to the value of the diamagnetic reference shift.[28] This correlation probably accounts for a significant part of the variance between the thermodynamic parameters obtained from the Cp and Cp* data sets for complex **5**. It also indicates that the values obtained from the Cp data are in general less susceptible to errors arising from approximate diamagnetic reference values.

Complexes **1**, **6**, and **8** exhibit linear isotropic shift vs $1/T$ behavior consistent with the Curie law. The possibility that these complexes are truly ground-state triplets cannot be ruled out from the NMR data alone, but consideration of the low symmetry (maximum C_{2v}) possible for all the trinuclear complexes excludes all but accidental orbital degeneracies. Low-temperature magnetic susceptibility measurements conclusively rule out a triplet ground state for complex **1**.[29] Thus, it is unlikely that any of these complexes are truly ground-state triplets.

Coupling Constants. The dipolar contributions to the isotropic shifts in several similar trinuclear complexes exhibiting pseudo-D_{3h} symmetry have been observed to be small.[2d,30] From MO studies the triplet states responsible for the paramagnetic shifts observed here should all be derived from a $^3A_2$ state under C_{2v} symmetry. If contact spin delocalization to the protons occurs predominantly through the Cp π-systems, then the well-known shift reversal effect should occur when a ring proton is replaced by a methyl group as in Cp*.[31] The best tests for this prediction are complexes **4** and **6**, where the metal ions are all the same but the number of Cp and Cp* rings is varied. In these and all other cases the signals for the Cp and Cp* protons are *both* shifted upfield ($K_i < 0$), contrary to the

(24) Holm, R. H.; Hawkins, C. J. In *NMR of Paramagnetic Molecules Principles and Applications*; La Mar, D. N., Horrocks, W. Dew, Jr., Holm, R. H., Eds.; Academic Press: New York, 1973; Chapter 7.

(25) A three-parameter (A_i, ΔH, and ΔS) nonlinear least-squares fit to the data was performed using a program written by M. Leitzke (Oak Ridge National Laboratories). The convergence criterion for a satisfactory fit to the data was a 0.1% change in any parameter of fit. Listed uncertainties in Table IX are 2 times the standard deviation calculated for each parameter.

(26) The paramagnetic shift is calculated according to the equation $\delta_{obsd} = \delta_{dia} - \delta_{para}$. (The sign of δ_{para} is opposite that of δ_{dia} and δ_{obsd}.) Although no diamagnetic shift reference compounds are known for the complexes **4** and **7**, the range of chemical shifts for diamagnetic complexes containing Cp ring and Cp* methyl protons may be approximated as 5 ± 0.5 and 2 ± 0.5 ppm, respectively. These numbers were used to estimate δ_{dia}. (See Table IX and text.)

(27) Adding an additional, linear offset to the shift data as a fit parameter gave disastrous results when in no case did any of the fits converge. A second approach involved adding a linear offset outside the least-squares routine. Convergence criteria in this case involved minimizing the overall standard deviation of the least-squares fit while independently varying the diamagnetic offset. Good, well-behaved convergence was observed in all cases for this model.

(28) In the case of complex **4**, least-squares fits were found to be extremely sensitive to an offset added to account for small errors in the measured diamagnetic position of the Cp* signal observed at low temperature. An offset of −0.08 ppm caused a 20% change in all fit parameters. An offset of +0.08 ppm caused the fit to diverge.

(29) In an earlier paper,[13a] it was stated incorrectly that the ground state for complex **1** was derived from a triplet state on the basis of NMR data alone. Magnetic susceptibility measurements indicate that the ground state for complex **1** is actually a singlet and that the paramagnetic shifts observed for **1** are derived from a spin equilibrium. Full details of magnetic susceptibility studies on these complexes will be reported in a future publication.

(30) (a) Frisch, P. D.; Dahl, L. F. *J. Am. Chem. Soc.* **1972**, *94*, 5082–5084. (b) Sorai, M.; Kosaki, A.; Suga, H.; Seki, S.; Yoshida, T.; Otsuka, S. *Bull. Chem. Soc. Jpn.* **1971**, *44*, 2364–2371.

(31) Horrocks, W. DeW., Jr. Chapter 4 of ref 20.

Scheme IV

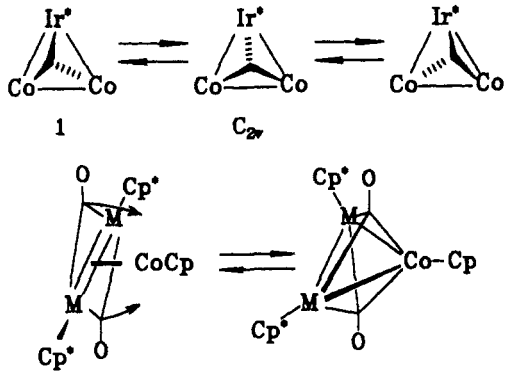

shift reversal prediction. Thus it appears that contact π-delocalization mechanisms are not the only important contributions to the isotropic shift and that σ-delocalization pathways must also be considered.[32,33]

Thermodynamic Parameters. The positive enthalpy figures listed in Table IX indicate that the singlet-state isomer is the lower energy isomer. Values of 18.1 kJ/mol and 50.2 J/(mol·K) have been reported for the enthalpy and entropy terms associated with the singlet $\rightleftarrows$ triplet equilibrium exhibited by the complex, $(Cp^*Co)_3(CO)_2$.[10c] The temperature dependence of the proton shifts for complex **5** is quite similar to this complex and, as expected, the enthalpy values are also similar. The enthalpy values for **4** and **7** are smaller, consistent with shifting the curve defined by eq 1 to lower temperature. Finally, complexes **1**, **6**, and **8** should exhibit even smaller enthalpy values than observed above assuming comparable entropy values.

The entropy changes may be divided into two parts: an $R(\ln 3)$ term that accounts for the different degeneracies of the singlet and triplet states,[34] and the remainder associated with any other changes that occur on isomerization.

Two structural isomerizations may be linked to the spin-state equilibria observed for these complexes. The first is a $\mu_2 \rightleftarrows \mu_3 \rightleftarrows \mu_2$ movement of the carbonyl ligands *across* the C_{2v} mirror plane in these complexes. This is known to occur in complex **1**[13a] (Scheme IV). The second involves a simple $\mu_2 \rightleftarrows \mu_3$ canting of the carbonyl ligands *within* this mirror plane as illustrated for the $*M_2Co$ series in Scheme IV.

The structural results section clearly shows that such changes in the carbonyl coordination geometry are accompanied by rather dramatic changes in the M–M bond distances. Theoretical studies (vide infra) indicate that either of the limiting geometries (edge-bridging vs triply bridging) may be the triplet-state isomer even though rigorous degeneracies are symmetry forbidden. The carbonyl ligands generally are observed in edge-bridging coordination modes in the solid state, but the triply bridging geometry does not appear to be separated from these structures by large energy barriers. We speculate that the more symmetrical μ_3 isomer, where the carbonyl ligands interact more equally with all three metals and the metal–metal separations are more nearly equal, is the triplet-state isomer. Magnetic susceptibility studies on the above complexes and ESR studies on the one-electron reduced, 47-electron analogues are in progress to gain further insight into this possibility.

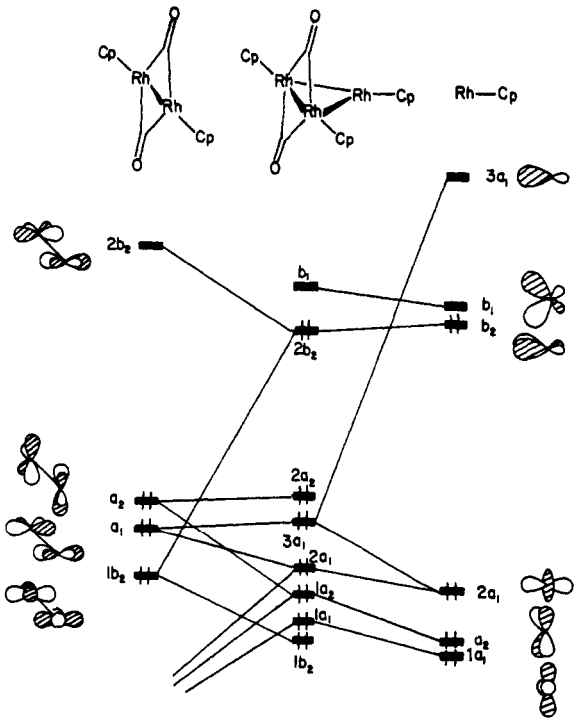

Figure 11. Molecular orbital correlation diagram from Pinhas et al.[3a] for the C_{2v} structure of $(Cp^*Rh)_3(CO)_2$ containing edge-bridging carbonyl ligands. Reproduced with permission.

Electronic Structure and Molecular Orbital Calculations. Several reports have appeared that model trinuclear clusters related to the ones discussed here.[3] In particular, Pinhas et al.[3a] have described a Walsh analysis of the approach to triply bridging coordination geometries of the carbonyl ligands in $Cp_3Rh_3(CO)_2$, starting from an edge-bridging geometry that is *identical with the structures observed for the complexes described here.*

The MO diagram[3a] for the C_{2v} (edge-bridging carbonyls) isomer of $Cp_3Rh_3(CO)_2$ is reproduced in Figure 11. The HOMO ($2b_2$) is composed primarily of in-plane metal d orbitals from both fragments. The MO contributed by the dinuclear fragment $[CpRh(\mu\text{-}CO)]_2$ is antibonding with respect to the Rh–Rh bond, while the CpRh fragment contributes essentially a d_{xz} orbital to this b_2 orbital. The LUMO (b_1) for the complex is derived solely from the CpRh fragment and is oriented perpendicular to the plane of the metals. The HOMO–LUMO set is well separated from both lower lying filled and higher lying orbitals. They are similar in energy and could explain the spin equilibria observed in these complexes. Strong support for the order shown is found in the character of the HOMO; in the isolated dinuclear complex, this b_2 orbital is metal–metal antibonding and unoccupied. If, in the formation of the trinuclear complex, the resulting MO derived from it is occupied, one clear prediction can be made: the metal–metal bond in the original dinuclear species should be weakened and thus elongated, *exactly as is observed in every instance where the carbonyls remain edge-bridging.* Therefore, the $2b_2$ orbital is occupied and is the HOMO for complexes exhibiting the edge-bridging carbonyl geometry. More insight into the interaction of these MOs is gained from the isolobal analogy of the dinuclear complex to an olefin. In this context the HOMO may be viewed as corresponding to the classic Dewar–Chatt–

(32) Olson et al.[10c] have reported that the corresponding hyperfine coupling constant for $(Cp^*Co)_3(CO)_2$ exhibits the opposite sign ($K_i > 0$) (downfield shift) in contrast to protons of the methyl groups of the Cp* ligands in the complexes described here.

(33) Detailed studies of the shift mechanisms of several metallocene derivatives concluded for the series Cp_2M, M = V, Cr, Co, and Ni, that the importance of σ-contact shifts grew for the later metals in the series. However, only qualitative agreement could be obtained between MO calculations and observed coupling constants in these studies. See, for example: (a) Rettig, M. F.; Drago, R. S. *J. Am. Chem. Soc.* **1969**, *91*, 1361–1370; (b) *Ibid.* **1969**, *91*, 3432–3441.

(34) Horrocks, W. DeW., Jr. *J. Am. Chem. Soc.* **1965**, *87*, 3779–3780.

Scheme V

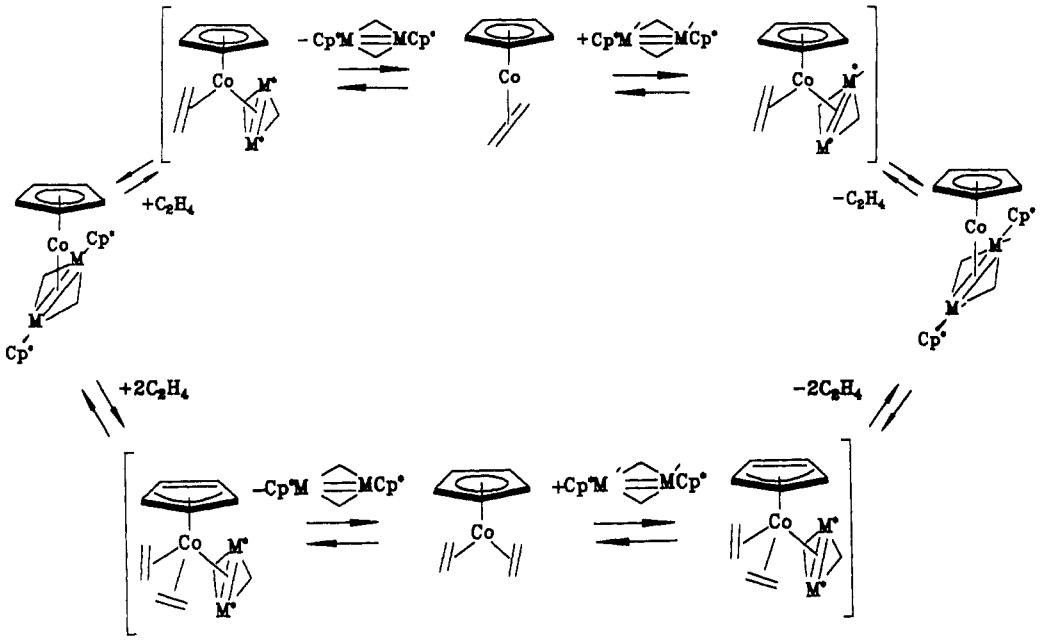

Duncanson model for back-bonding between a CpM fragment and an olefin.

For the triply bridging geometry, the situation is quite different. The complexes described here cannot attain the high symmetry (C_{3v}) possible in the case of the trirhodium species. Thus, the doubly degenerate e levels[3a] associated with this geometry will not be strictly applicable here. An important difference between the edge-bridging and triply bridging geometries is the length of the metal–metal bond in the original dinuclear species. In complex **7** the Rh–Rh distance is virtually identical with that observed in the original dinuclear precursor. This behavior is also predicted by calculations done on the C_{3v} isomer of the trirhodium species (correlation diagram not shown). As the carbonyls tilt over the M_3 triangle, the original b_2 HOMO for the C_{2v} geometry drops in energy and becomes one of the components of an e′ set for the C_{3v} geometry. It also loses the pronounced antibonding character responsible for the lengthening of the M–M bond as considerable carbonyl character mixes in. The only metal-based MO for the C_{3v} geometry that is M–M antibonding is the a_2 orbital, which is predicted to be unoccupied in these complexes. Thus, the changes in M–M distances observed between complex **7** with triply bridging carbonyls and all the other complexes in these series are supported by these calculations.

It is also possible to make a number of chemical predictions based on the above discussion. For the edge-bridging geometry, the isolabal analogy between these complexes and a 16-electron Cp(*)M(olefin) species has been pointed out. Such a species would be expected to react with a variety of two-electron ligands to satisfy its electron deficiency corresponding either to a 46-electron cluster count or to a mononuclear 16-electron count. This is observed; all of the complexes react instantly with carbon monoxide to form saturated tricarbonyl adducts. Reaction of any of the title complexes with ethylene causes fragmentation to the cobalt bisethylene complex and the familiar dinuclear species, again consistent with the picture presented above.

Dinuclear Exchange Reactions. The fragmentation reaction with ethylene presumably occurs through stepwise coordination of ethylene by the unsaturated complex, followed by essentially the reverse set of steps involved in their formation. From our synthetic studies it is clear that the bisethylene species $CpCo(C_2H_4)_2$, once formed, would readily react with any other unsaturated dinuclear species present. When taken together, these observations present the opportunity of exchanging one dinuclear fragment for another at a CpCo center.

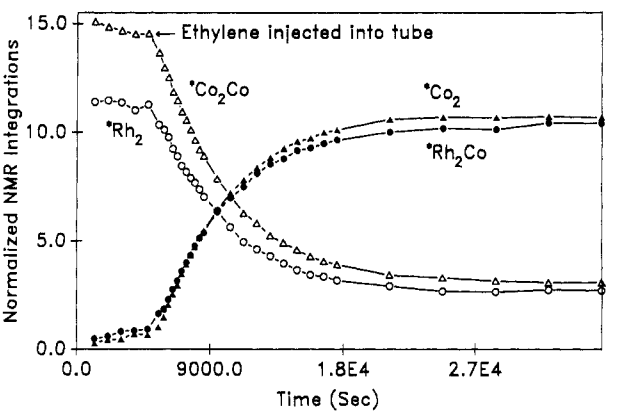

Figure 12. Effect of ethylene as a catalyst on the exchange of dinuclear fragments $[Cp^*Rh(\mu\text{-}CO)]_2$ and $[Cp^*Co(\mu\text{-}CO)]_2$ between trinuclear complex **6** and **7** (solvent C_6D_6; T = 22 °C).

No reaction is observed (NMR, C_6D_6, THF-d_8) when members of the $^*M_2Co$ series are exposed to either of the cobalt or rhodium dinuclear complexes $[Cp^*M(\mu\text{-}CO)]_2$. Subsequent experiments spiked with a small amount of ethylene showed an immediate acceleration in rate as the reaction proceeded smoothly to an equilibrium point. The effect of the addition of ethylene to a mixture of complex **6** and $[Cp^*Rh(\mu\text{-}CO)]_2$ is shown in Figure 12. Before ethylene is introduced into the NMR tube, little evidence of reaction is observed.[35] Immediately afterwards, rapid equilibration of all species involved in the exchange is observed. The reaction is *catalyzed* either by free ethylene or by the cobalt bisethylene complex **2**. Identical equilibrium distributions of products are obtained when these reactions are run in the forward or reverse directions. Preliminary mechanistic studies indicate that the rate law is second-order overall and first-order with respect to either

(35) Trace amounts of $Cp(C_2H_4)_2$ as an impurity in the trinuclear starting material are responsible for the small amounts of exchange products before the addition of ethylene.

Scheme VI

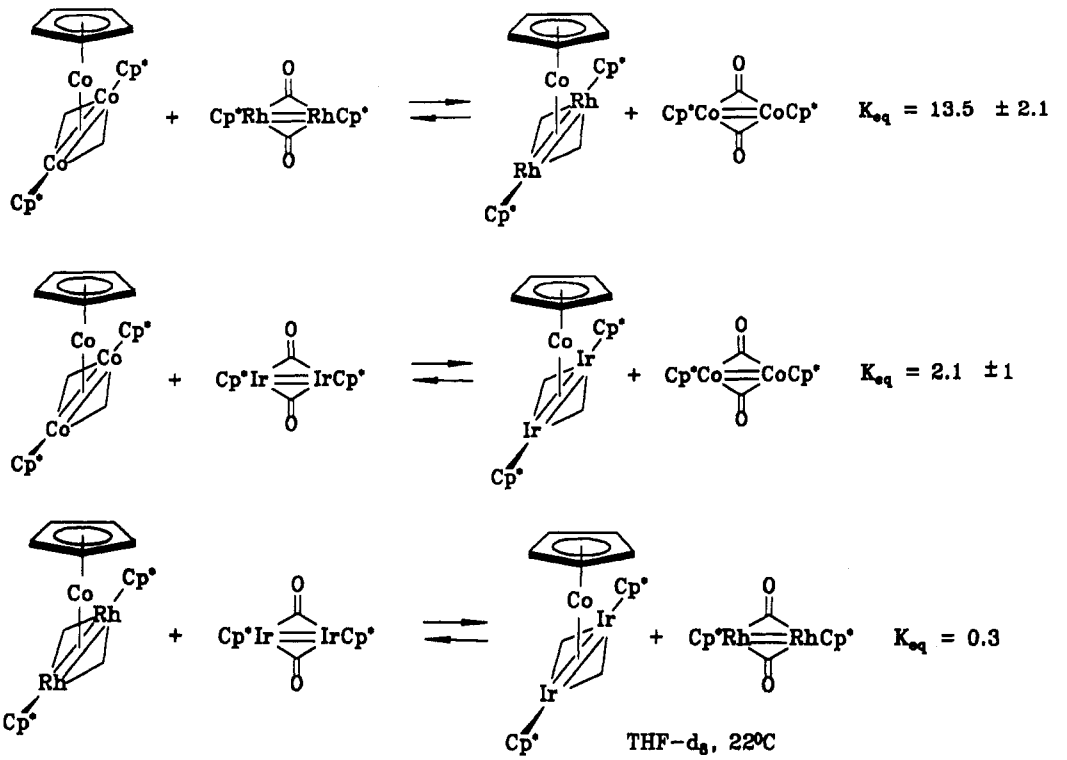

starting complex. Two mechanisms consistent with these observations are shown in Scheme V.

Reaction is initiated by coordination of ethylene to the CpCo center.[36] Two distinct pathways are now possible. Loss of the dinuclear species produces one of the final products and a transient, unsaturated CpCo(ethylene) species.[37] This intermediate is then trapped by either the original dinuclear complex or any other dinuclear complex present, eventually leading to the final trinuclear product. Alternately, a second molecule of ethylene could coordinate to the cobalt center before the dinuclear species is lost. Coordination of an extra ligand may be facilitated by slippage of the cyclopentadienyl ring from an η^5- to η^3-coordination mode to preserve the formal 18-electron count around the metal. Loss of the dinuclear species should then occur quite readily, generating the bisethylene complex, which can then react further with either dinuclear complex in the reaction mixture. Precedent for either the "dissociative" or "associative" reaction pathways for the CpCo moiety is known.[38] Within the $CpCo[Cp^*M(\mu\text{-}CO)]_2$ series complex **7** appears to be favored over either **6** or **8**, but not greatly. Equilibrium constants are summarized in Scheme VI.

The exchange reactions for the M^*Co_2 series (complexes **1**, **4**, and **5**) are more complicated than those described above. In addition to liberating $[CpCo(\mu\text{-}CO)]_2$, several other species are observed that indicate not only that dinuclear exchange is occurring involving trinuclear species but also dinuclear metathesis products are observed, along with unanticipated trinuclear complexes. These reactions will be reported on at a later time along with both kinetic and thermodynamic details of the exchange reactions described above.

Although these exchange reactions have been described within the context of supporting a model for the electronic structure of these complexes, there is a more far-reaching aspect to these reactions. The addition to or exchange of polynuclear fragments from an unsaturated mononuclear center is one of the fundamental cluster building and degradation reactions. Much insight into this process is gained with the isolobal analogies described above. Direct metal–metal bonding interactions dominate the overall interaction of these two fragments. An important constituent of this interaction has been identified as the HOMO for these complexes which involves a net back-bonding type donation from the CpCo moiety to an unfilled MO associated with the $[Cp^*M(\mu\text{-}CO)]_2$ fragment. The fluxional behavior of the carbonyl ligands around the metal core is linked to the stretching and contraction of the various metal–metal bonds. The energy differences and barriers between the μ_2- and μ_3-coordination modes for the carbonyl ligands appear to be small in these complexes, as complex **7** is not excluded from participation in these dinuclear exchange equilibria because of its triply bridging carbonyl ligands. Investigations are now focused on determining the relative importance of these two factors, as well as the generality of these exchange interactions with other organometallic species.

Summary and Conclusions

The synthesis and properties of two new series of trinuclear complexes were described. These 46-valence-electron cluster complexes exhibit paramagnetically shifted ^1H NMR spectra, the temperature dependence of which is consistent with a spin-state equilibrium involving ground-state singlets and low-lying triplet state isomers. NMR and structural data suggest that these spin-state equilibria are linked together with fluxional behavior of the carbonyl ligands. The solid-state structures also indicate that carbonyl movements between edge-bridging and triply bridging coordination geometries are linked with large changes in the separations between metal atoms within the trimetal core. Both the structural and spin-state

(36) Steric interactions presumably destabilize pentanuclear intermediates that might be formed through the direct reaction of the trinuclear and dinuclear starting complexes.

(37) This species may or may not have a labile solvent molecule coordinated to the cobalt atom.

(38) Janowicz, A. H.; Bryndza, H. E.; Bergman, R. G. *J. Am. Chem. Soc.* **1981**, *103*, 1516–1518.

changes may be rationalized by analogy to an unsaturated 16-electron olefin complex of the form Cp*M(olefin). The olefin equivalent is identified as the dinuclear fragment containing the edge-bridging carbonyls within the trinuclear structure. On the basis of this model, the HOMO for these complexes corresponds to a net transfer of electron density from the $Cp^{(*)}M$ fragment into a metal-centered antibonding orbital of the dinuclear fragment. Further support for this model is garnered from dinuclear exchange reactions catalyzed by ethylene.

Experimental Section

Materials. All solvents used in the preparation and manipulation of the title complexes were reagent grade and were distilled under dinitrogen from Na/K alloy (hexane, toluene, diethyl ether, THF) or calcium hydride (methylene chloride). Much of the air-sensitive work was carried out in an inert atmosphere (argon or helium) drybox, (Innovative Technologies, MB-150). The oxygen content was periodically monitored by using an Innovative Technologies oxygen analyzer. An oxygen content of less than 10 ppm was maintained during all reactions. Reactions performed outside of the box were run using Schlenk techniques under purified dinitrogen (MnO on vermiculite followed by activated 4-Å sieves). Chromatographic separations were carried out under anaerobic and anhydrous conditions using jacketed flash chromatography columns. The separation medium was silica gel that was degassed by at least five vacuum–nitrogen cycles over two days. Columns were prepared in hexane, and the solvent polarity increased as the constituents were eluted. Air-sensitive compounds that did not need refrigeration were stored in the dry box. Air-sensitive compounds requiring refrigeration were stored in Schlenk vessels under an inert atmosphere at 2 or −25 °C.

Physical Measurements. Nuclear magnetic resonance (NMR) spectra were recorded on JEOL FX90Q (90 MHz) or a Nicolet NT-200 (200MHz) Fourier transform instrument. Chemical shifts were referenced to the residual proton signal of the following deuterated solvents: $\delta(C_6D_5H)$ 7.15; $\delta(C_7D_7H)$ 2.09 (methyl quintet); δ(THF-d_7H) 3.58 or 1.73; $\delta(CHCl_3)$ 7.26 ppm. Because of the existence of two sign conventions in the reporting of chemical shift values for paramagnetic compounds, it should be noted that proton shifts reported here that are above TMS (high field) are negative. Infrared (IR) spectra were recorded on either a Perkin-Elmer 1330 spectrophotometer or a Digilab FTS-20E FTIR spectrometer. Infrared spectra were referenced to polystyrene, 1601.4 cm^{-1}. Elemental analyses were performed by Desert Analytics—Organic Microanalysis of Tucson, AZ.

Syntheses. The following complexes were synthesized according to literature procedures: Cp*-H;[39] $[Cp^*IrCl(\mu\text{-}Cl)]_2$;[40] $[Cp^*RhCl(\mu\text{-}Cl)]_2$;[41] $[Ir(C_8H_{14})_2(\mu\text{-}Cl)]_2$;[42] Cp_2Co;[43] $Cp^*Ir(CO)_2$;[2,44] $Cp^*Co(CO)_2$;[2a] $Cp^*Rh(CO)_2$;[45] $[Cp^*Co(\mu\text{-}CO)]_2$;[46] $[Cp^*Rh(\mu\text{-}CO)]_2$.[47]

Bis(μ-carbonyl)bis(pentamethylcyclopentadienyl)diiridium, $[Cp^*Ir(\mu\text{-}CO)]_2$.[48] *Caution!* This reaction evolves carbon monoxide and should be attempted only in a well-ventilated fume hood. In a minimum of 1-butanol (2 mL), 0.15 g (0.4 mmol) of $Cp^*Ir(CO)_2$ was heated under nitrogen to 150 °C with vigorous stirring. The solvent, initially yellow due to $Cp^*Ir(CO)_2$ became colorless after 3 days. After 4 days, heating was discontinued, and the solvent removed under vacuum. The residue was dissolved in hot hexane, filtered through glass wool, and cooled to −25 °C. The microcrystalline product was isolated and dried to give 0.06 g (43%). ^1H NMR (C_6D_6, 25 °C) δ 1.578 (s); (toluene-d_8, 25 °C) δ 1.599 (s); (THF-d_8) δ 1.740 (s); IR (KBr) ν(CO) 1685 (s), (toluene) 1688 (s), (CH_2Cl_2) 1672 (s), (benzene) 1685 (s), (hexane) 1701 (s), (THF) 1692 (s) cm^{-1}.

General Procedure for the Preparation of the Trinuclear Complexes 1 and 4–8. In an inert-atmosphere box separate solutions of the carbonyl-containing starting material in ether (approximately 100 mg in 30 mL) and the bisethylene complex, $CpCo(C_2H_4)_2$, in approximately 50 mL of hexane are prepared. The amount of the bisethylene complex used in each reaction was always in slight excess (0.5 equiv) of the number of "CpCo" equivalents required by the reaction stoichiometry. The ether solution of the carbonyl complex was added portionwise to the hexane solution over 15 min. Immediate reaction was noted by color changes (orange to dark green or brown). Several times during the addition the reaction flask was capped and exposed to vacuum briefly with vigorous stirring. After the additions were complete, the volume of the solution was reduced to between 10 and 20 mL, at which time a microcrystalline precipitate was observed. The solid was collected by filtration, washed with hexane, and dried under vacuo. Yields of the crude products (>95% pure) are typically between 60 and 90% on scales of 0.1 and 1.0 g. Recrystallization from hot hexane yields analytically pure materials or single crystals for X-ray diffraction analysis.

[Bis(μ-carbonyl)bis(cyclopentadienyl)dicobalt](pentamethylcyclopentadienyl)iridium, $(\eta^5\text{-}C_{10}H_{15})Ir(\mu\text{-}CO)_2Co_2(\eta^5\text{-}C_5H_5)_2$ (1). The preparation and characterization of this complex starting from the dinuclear complex $Cp^*Ir(\mu\text{-}CO)_2CoCp$ have already been reported.[13a] Starting from the $Cp^*Ir(CO)_2$ the yield is 0.949 g (83%).

[Bis(μ-carbonyl)bis(cyclopentadienyl)dicobalt](pentamethylcyclopentadienyl)cobalt, $(\eta^5\text{-}C_5Me_5)Co(\mu\text{-}CO)_2Co_2(\eta^5\text{-}C_5H_5)_2$ (4). Yield on a 0.215-g scale ($Cp^*Co(CO)_2$) 0.400 g (94%). ^1H NMR (C_6D_6, 24 °C) δ −2.24 (s, 15 H), −11.25 (s, 10 H); (toluene-d_8, 23 °C) δ −2.14 (s, 15 H), −11.051 (s, 10 H); (THF-d_8, 24 °C) δ −2.108 (s, 15 H), −11.443 (s, 10 H); IR (KBr) ν(CO) 1699 (s), (THF) 1707 (s), (hexane) 1695 (s), (CH_2Cl_2) 1688 (s), (benzene) 1702 (s) cm^{-1}. Anal. Calcd for $C_{22}H_{25}Co_3O_2$ (498.24): C, 53.05; H, 5.06. Found: C, 52.99; H, 5.06.

[Bis(μ-carbonyl)bis(cyclopentadienyl)dicobalt](pentamethylcyclopentadienyl)rhodium, $(\eta^5\text{-}C_5Me_5)Rh(\mu\text{-}CO)_2Co_2(\eta^5\text{-}C_5H_5)_2$ (5). Yield on a 0.300 g scale ($Cp^*Rh(CO)_2$) 0.520 g (93%). ^1H NMR (C_6D_6, 24 °C) δ 3.61 (s, 10 H), 0.31 (s, 15 H); (toluene-d_8, 23 °C) δ 3.70 (s, 10 H), 0.43 (s, 15 H); (THF-d_8, 25 °C) δ 3.67 (s, 10 H), 0.76 (s, 15 H); IR (KBr) ν(CO) 1701 (s); (THF) 1705 (s); (CH_2Cl_2) 1675 (s); (benzene) 1702 (s) cm^{-1}. Anal. Calcd for $C_{22}H_{25}Co_2O_2Rh$ (542.21): C, 48.73; H, 4.65. Found: C, 48.73; H, 4.77.

[Bis(μ-carbonyl)bis(pentamethylcyclopentadienyl)dicobalt]cyclopentadienylcobalt, $(\eta^5\text{-}C_5Me_5)_2Co_2(\mu\text{-}CO)_2Co(\eta^5\text{-}C_5H_5)$ (6). Yield on a 0.20-g scale ($[Cp^*Co(\mu\text{-}CO)]_2$) 0.240 g (94%). ^1H NMR (C_6D_6, 24 °C) δ −7.79 (s, 30 H), −55.42 (s, 5 H); (toluene-d_8, 22 °C) δ −7.28 (s, 30 H), −56.12 (s, 5 H); (THF-d_8, 25 °C) δ −7.00 (s, 30 H), −55.60 (s, 5 H); IR (KBr) ν(CO) 1703 (w), 1686 (s); (THF) 1698 (s); (CH_2Cl_2) 1690 (s) cm^{-1}. Anal. Calcd for $C_{27}H_{35}Co_3O_2$ (568.37): C, 57.06; H, 6.21. Found: C, 56.83; H, 6.33.

[Bis(μ-carbonyl)bis(pentamethylcyclopentadienyl)dirhodium](μ-cyclopentadienyl)cobalt, $(\eta^5\text{-}C_5Me_5)_2Rh_2(\mu\text{-}CO)_2Co(\eta^5\text{-}C_5H_5)$ (7). Yield on a 0.30-g scale ($[Cp^*Rh(\mu\text{-}CO)]_2$) 0.38 g (76%). ^1H NMR (C_6D_6, 24 °C) δ −10.83 (s, 30 H), −41.93 (s, 5 H); (toluene-d_8, 23 °C) δ −11.34 (s, 30 H), −44.07 (s, 5 H); (THF-d_8, 25 °C) δ −10.89 (s, 30 H), −42.71 (s, 5 H); IR (KBr) ν(CO) 1690 (s); (THF) 1692 (s); (CH_2Cl_2) 1680 (s); (benzene) 1688 (s) cm^{-1}. Anal. Calcd for $C_{27}H_{35}CoO_2Rh_2$ (656.32): C, 49.41; H, 5.37. Found: C, 49.13; H, 5.41.

[Bis(μ-carbonyl)bis(pentamethylcyclopentadienyl)diiridium]cyclopentadienylcobalt, $(\eta^5\text{-}C_5Me_5)_2Ir_2(\mu\text{-}CO)_2Co(\eta^5\text{-}C_5H_5)$ (8). Yield on a 0.06-g scale ($[Cp^*Ir(\mu\text{-}CO)]_2$) 0.056 g (80%). ^1H NMR (C_6D_6, 23 °C) δ −23.02 (s, 30 H), −72.49 (s, 5 H); (toluene-d_8, 24 °C) δ −23.99 (s, 30 H), −72.70 (s, 5 H); (THF-d_8, 22 °C) δ −24.09 (s, 30 H), −73.12 (s, 5 H); IR (KBr) ν(CO) 1900

(39) Threlkel, R. S.; Bercaw, J. E. *J. Organomet. Chem.* **1977**, *136*, 1–5.
(40) Kang, J. W.; Moseley, K.; Maitlis, P. M. *J. Am. Chem. Soc.* **1969**, *91*, 5970–5977.
(41) Booth, B. L.; Haszeldine, R. N.; Hill, M. *J. Chem. Soc. A* **1969**, 1299–1303.
(42) Onderlinden, A. L.; van der Ent, A. *Inorg. Chim. Acta* **1972**, *6*, 420–426.
(43) Wilkinson, G.; Cotton, F. A.; Birmingham, J. M. *J. Inorg. Nucl. Chem.* **1956**, *2*, 95–113.
(44) Guggolz, E.; Ziegler, M. L. *Z. Naturforsch.* **1981**, *36b*, 1053–1059.
(45) Kang, J. W.; Maitlis, P. M. *J. Organomet. Chem.* **1971**, *26*, 393–399.
(46) Bailey, Jr., W. I.; Collins, D. M.; Cotton, F. A.; Baldwin, J. C.; Kaska, W. C. *J. Organomet. Chem.* **1979**, *165*, 373–381.
(47) Nutton, A.; Maitlis, P. M. *J. Organomet. Chem.* **1979**, *166*, C21–C22.
(48) Heinekey, D. M. Personal communication, Yale University.

(m), 1685 (s); (CH_2Cl_2) 1888 (s), 1665 (s); (toluene, 25 °C) 1902 (s), 1686 (s); (toluene, −78 °C) 1902 (s), 1686 (s); (THF) 1900 (s), 1680 (s); (hexane) 1910 (s), 1690 (s) cm^{-1}. Anal. Calcd for $C_{27}H_{35}CoIr_2O_2$ (834.94): C, 38.84; H, 4.22. Found: C, 39.12; H, 4.35.

Dinuclear Exchange Reactions. All reactions were conducted in flame-sealed NMR tubes. Deuterated NMR solvents (dried over Na/K alloy) were vacuum transferred into the NMR tube. All reaction mixtures were kept frozen at −196 °C until immediately before spectral measurements were made. Qualitative kinetic studies were obtained by using the KINET program (Nicolet). The first spectrum in each experiment was taken less than 5 min after the solvent was thawed and the KINET program initiated. All reactions were run at ambient temperature (22 °C).

X-ray Crystal Structure Determinations. Crystal data for **4–8** are collected in Table II. Minimally air-sensitive, brown-black crystals of **4–8** were recrystallized from hexane and mounted on glass fibers with epoxy resin. Unit-cell parameters were determined through least-squares refinement of the angular settings for 25 reflections ($18° \leq 2\theta \leq 25°$). Data were collected on a Nicolet R3m diffractometer with a graphite monochromator (λ(Mo Kα) = 0.710 73 Å). An empirical absorption correction (six reflections, Ψ scans, 216 data) was applied to the data for **4** and **6–8**. An additional correction for a linear 4% decay in reflection intensity was applied to the data for **8**.

Solution and Structure Refinement. Structures **4–6** were solved by direct methods (SOLV) that located the heavy atoms; **7** was solved by using the heavy-atom coordinates of the isomorphous structure, **6**. Locations of the remaining non-hydrogen atoms in **4–7** were determined through subsequent difference Fourier analyses and least-squares refinement. In **4**, a crystallographic 2-fold axis containing Co(1) and the midpoint of the Co(2)–Co(2a) bond produces disorder in the Cp* ring that could be resolved only as two nearly superimposed rings with slightly different centroids, although the limits of resolution sugest that this may be only artifactual. All non-hydrogen atoms in **4** and **5** were refined anisotropically with Cp hydrogen atoms calculated and fixed ($U = 1.2U$(adjacent C atom), d(C–H) = 0.96 Å).

The systematic absences for **6** and **7** determine four orthorhombic space groups—centrosymmetric *Ccmm* and noncentrosymmetric $Ccm2_1$, *Cc2m* and $C222_1$. Of the four space groups, only in *Ccmm* (nonstandard setting of *Cmcm*) could all of the non-hydrogen atoms be located and refined. Both structures **6** and **7** display disorder in the Cp and Cp* rings, the disorder consisting of interpenetrating rings due to two mutually perpendicular crystallographic mirror planes. Although never reaching a fully satisfactory model for the disorder due to limits of resolution, a recognizable pattern of superimposed Cp and Cp* rings were modeled with allowances for occupancies different from site location due to superimposed, or nearly superimposed, atom positions. None of the alternative space groups provided relief from the disorder. All metal atoms and carbonyl group atoms in **6** and **7** were refined anisotropically, but due to the structural disorder many of the Cp and Cp* carbon atoms were refined only isotropically. Also due to the disorder, hydrogen atoms were ignored in **6** and **7**.

The structure of **8** was solved via a Patterson map that located the Ir and Co atoms. Remaining atoms were located through subsequent difference Fourier syntheses and least-squares refinement. Systematic absences in the data defined either of orthorhombic space groups *Pnma* or $Pn2_1a$; the former, centrosymmetric alternative was initially suggested by the presence of mirror plane symmetry. The compound crystallizes as two independent half-molecules ($Z = 8$), each situated on a crystallographic mirror plane. In the first molecule (A) the plane contains the metal atoms, while in the second molecule (B) the plane bisects the Ir–Ir bond and Co atom. Rotational disorder is observed in the Cp ring attached to Co(1) of molecule A. This disorder is seen in the form of coplanar but not fully coaxial Cp rings. Attempts to model this disorder were not completely successful and resulted in constraining the Cp and Cp* rings to rigid, planar pentagons. Non-hydrogen atoms were refined anisotropically except for C(7), C(10), C(12)–C(21), C(24), C(27), C(33), and C(35); hydrogen atoms were ignored.

All computer programs used were from the P3 (Nicolet XRD, Madison, WI) and SHELXTL (G.M. Sheldrick, 1984) program libraries.

Figures 4–9 show the structures and numbering schemes for **4–8**, respectively. All thermal ellipsoids are drawn at the 40% level. The dotted lines denote unusually long metal atom–carbonyl interactions in **4–6** and **8**. Figure 10 shows a packing diagram of the two independent molecules in the unit cell of **8**.

Acknowledgment is made to the donors of the Petroleum Research Fund, administered by the American Chemical Society, for partial support of this research. We are grateful to the Johnson Matthey Co. for their generous loan of precious metal starting materials for this research.

Supplementary Material Available: Tables of atomic coordinates, complete bond lengths and angles, anisotropic thermal parameters, and hydrogen atom coordinates (36 pages); tables of observed and calculated structure factors (54 pages). Ordering information is given on any current masthead page.